Electronic Supplementary Material (ESI) for New Journal of Chemistry.

Hydroxylated 3-(pyridin-2-yl)coumarins as radical scavengers with potent lipoxygenase inhibitor activity

Sebastiano Masuri[1], Maria Grazia Cabiddu[1], Enzo Cadoni[1], Tiziana Pivetta[1]*

[1] Dipartimento di Scienze Chimiche e Geologiche, Università degli Studi di Cagliari, Cittadella Universitaria, 09042 Monserrato CA – Italy

SUPPLEMENTARY INFORMATION

Table of contents:

1. Spectral data

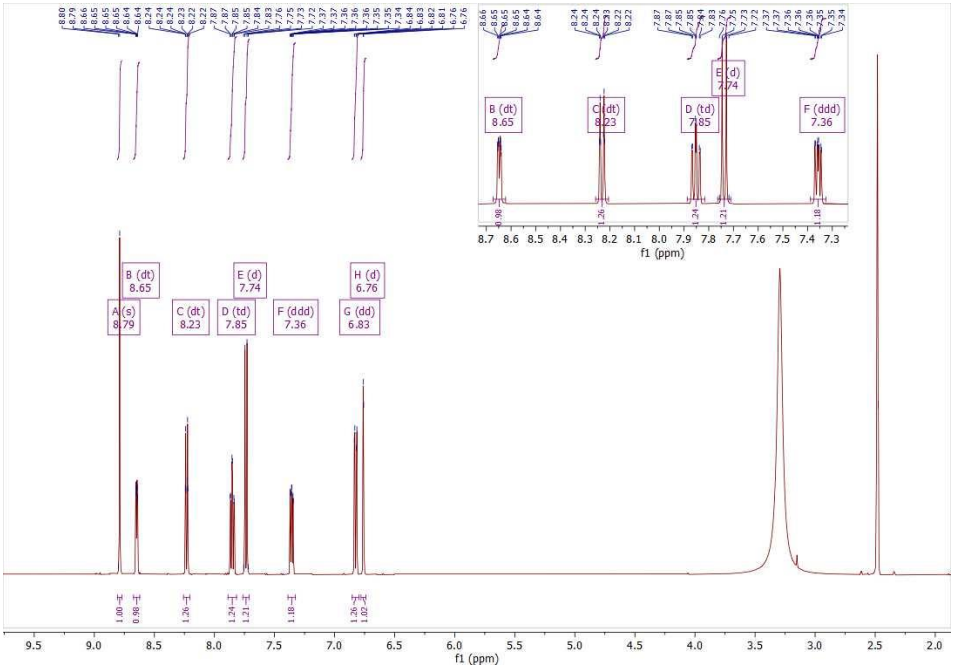

Fig. S1. ^{1}H NMR of ligand **2**, 7-Hydroxy-3-(pyridin-2-yl)-2*H*-chromen-2-one (500 MHz, DMSO-d_6).

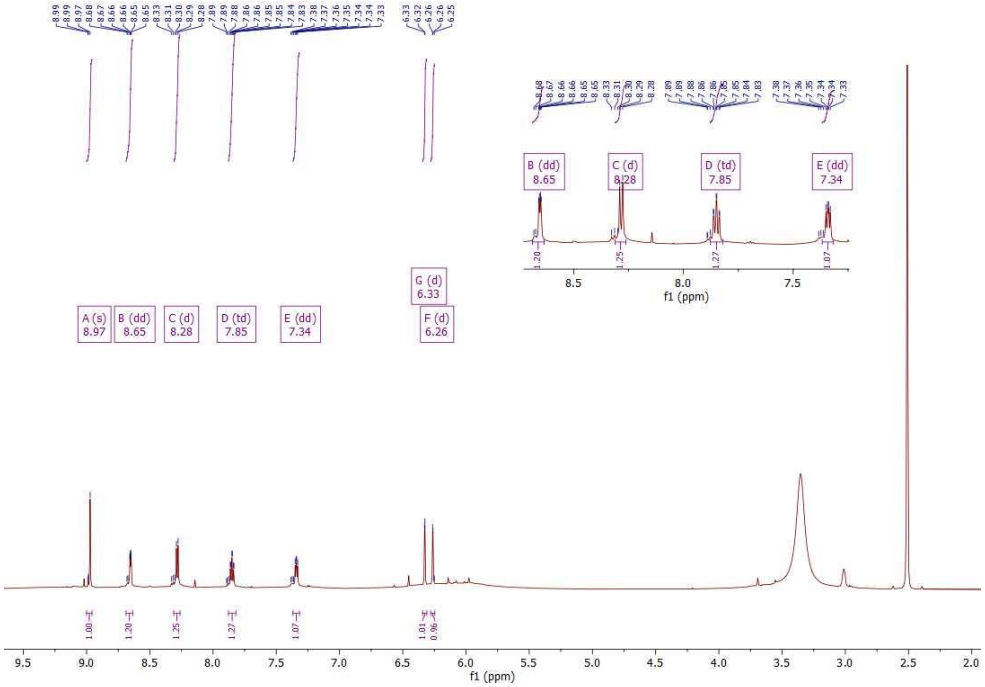

Fig. S2. ^{1}H NMR of ligand **3**, 5,7-dihydroxy-3-(pyridin-2-yl)-2*H*-chromen-2-one (600 MHz, DMSO-d_6).

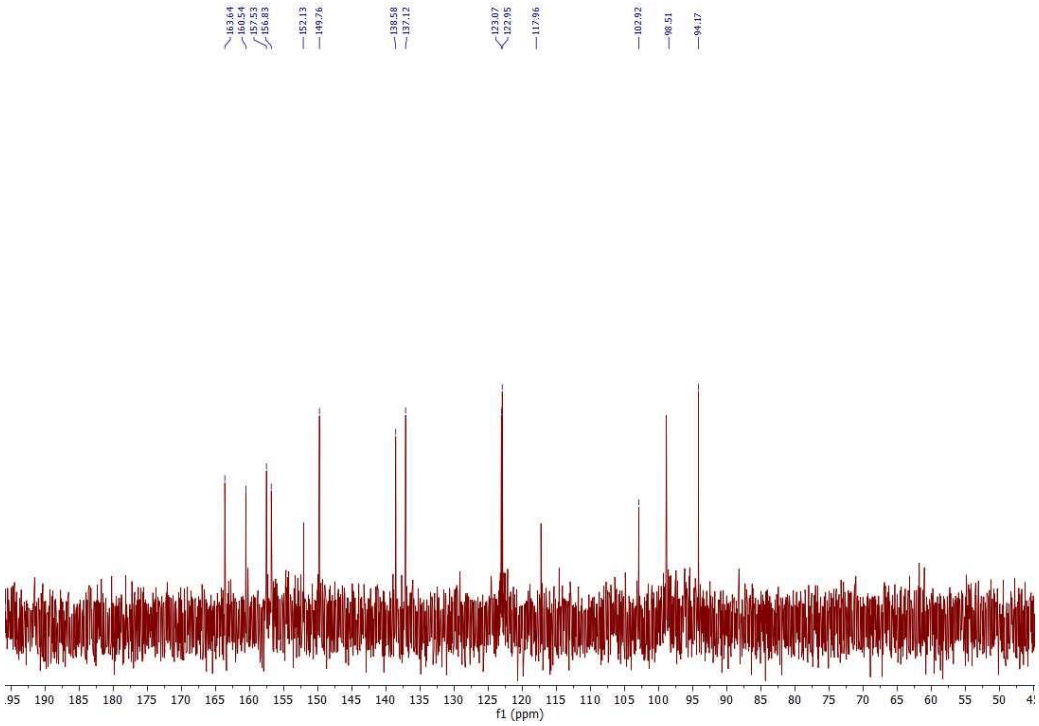

Fig. S3. ^{13}C NMR of ligand **3**, 5,7-dihydroxy-3-(pyridin-2-yl)-2*H*-chromen-2-one (158 MHz, DMSO-d_6).

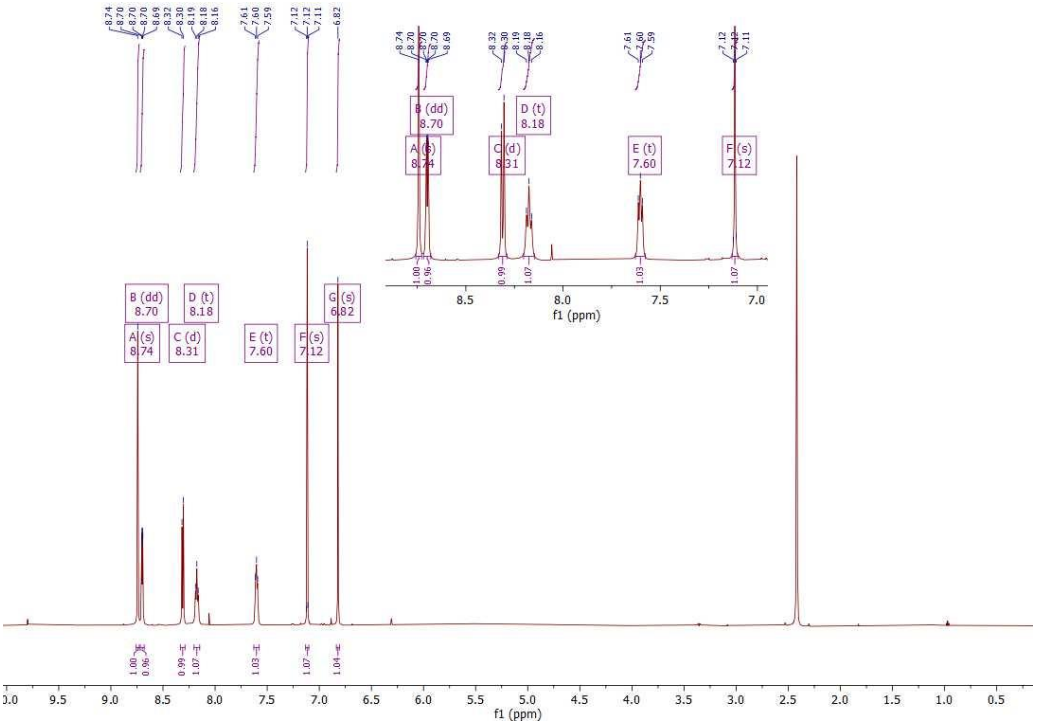

Fig. S4. ^{1}H NMR of ligand **4**, 6,7-dihydroxy-3-(pyridin-2-yl)-2*H*-chromen-2-one (600 MHz, DMSO-d_6).

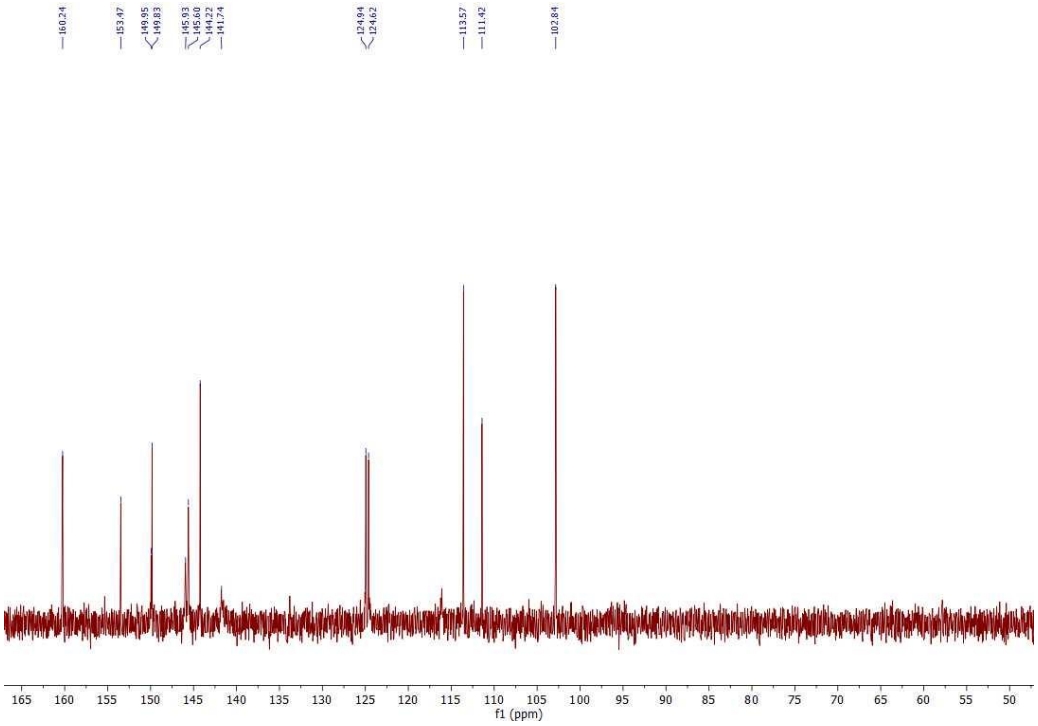

Fig. S5. ^{13}C NMR of ligand **4**, 6,7-dihydroxy-3-(pyridin-2-yl)-2*H*-chromen-2-one (158 MHz, DMSO-d_6).

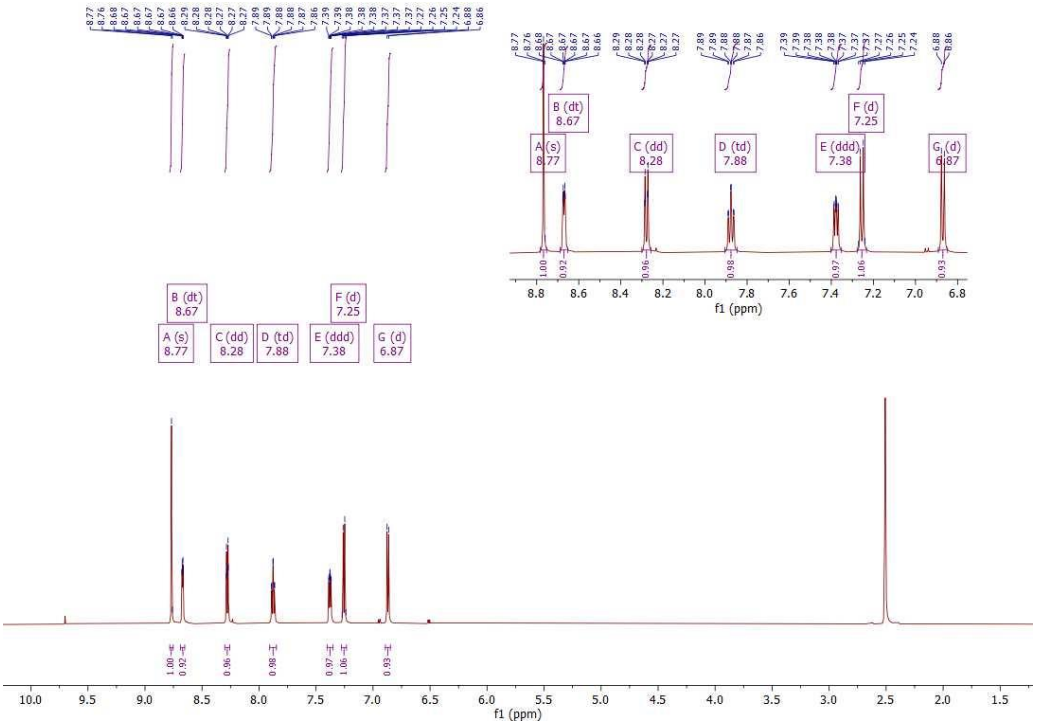

Fig. S6. ^{1}H NMR of ligand **5**, 7,8-dihydroxy-3-(pyridin-2-yl)-2*H*-chromen-2-one (600 MHz, DMSO-d_6).

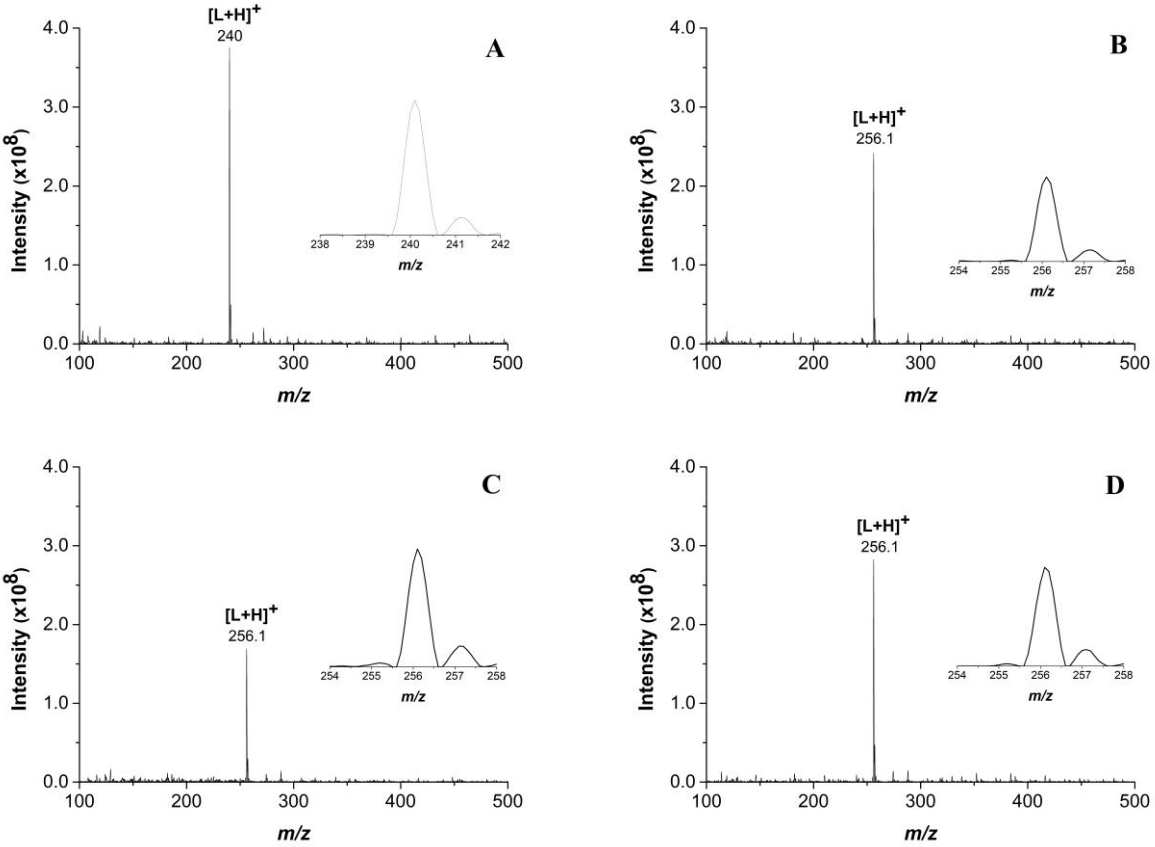

Fig. S7. ESI-MS spectra of **2** (**A**), **3** (**B**), **4** (**C**), **5** (**D**).

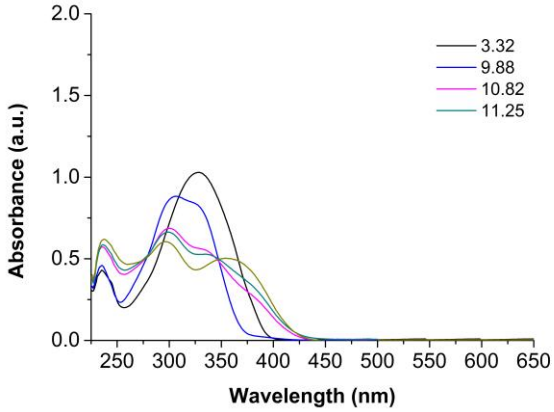

Fig. S8. UV-Vis spectra of **1** at pH > 10 (spectra at pH 3.32 and 9.88 are shown for comparison).

2. Spectrophotometric titrations

Spectral variations observed during the titration of 1

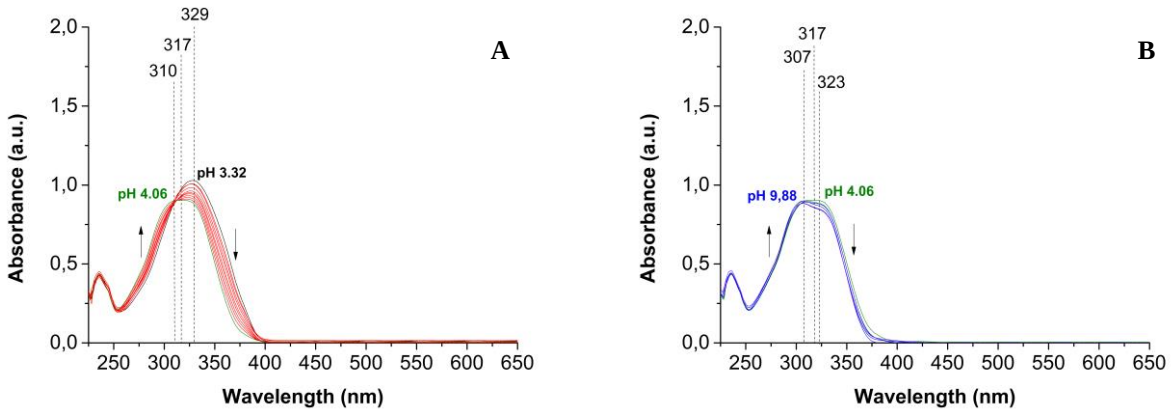

Fig. S9. Selected spectra collected during the potentiometric and spectrophotometric titration of **1** (1.26×10^{-4} M, 0.1 M NaCl, *t* 25°C, optic path length 0.5 cm) from pH 3.32 to 4.06 (**A**); from pH 4.06 to 9.88 (**B**).

During the titration with NaOH, three equilibria were evidenced in the pH range 3.32-9.88. At pH 3.32 a peak at 329 nm was present, while at increasing pH a decrease of the absorbance, with a blue-shift and the formation of an isosbestic point at 310 nm was observed. At pH 4.06 a larger band at 317 nm was formed (**Fig. S9A**) and further additions of NaOH determined a small decrease in absorbance and a change of the spectral shape (two overlapped peaks at 307 and 323 nm, **Fig. S9B**).

Spectral variations observed during the titration of 2

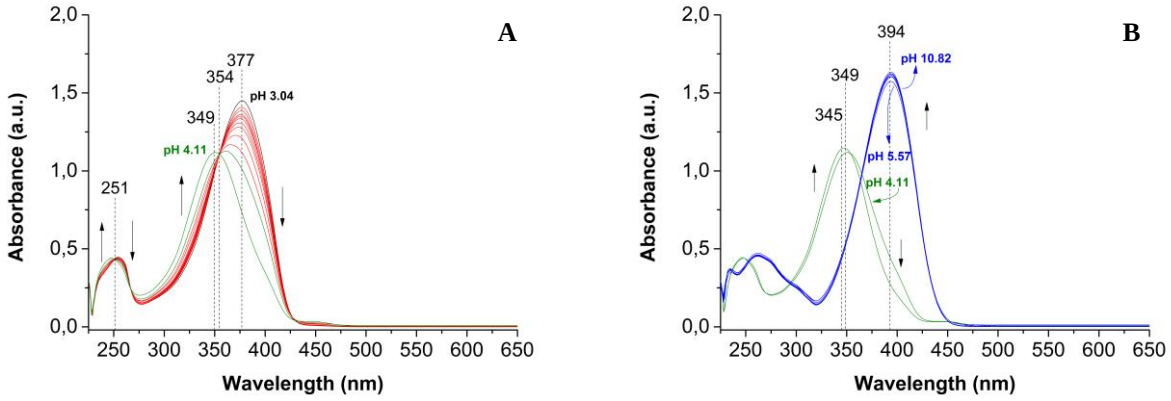

Fig. S10. Selected spectra collected during the potentiometric and spectrophotometric titration of **2** (1.24×10^{-4} M, 0.1 M NaCl, *t* 25°C, optic path length 0.5 cm from pH 3.04 to 4.11 (**A**); from pH 4.11 to 10.82 (**B**).

The analysis of the spectra recorded during the titration of **2** (pH range 3.04-10.82) evidenced the presence of four equilibria. At pH 3.04 a peak at 377 nm was observed. At higher pH a gradual decrease in absorbance and the formation of an isosbestic point at 354 nm were observed. Towards pH 4, the formation of a new band centred at 349 nm and the appearance of an additional isosbestic point at 251 nm were put in evidence (**Fig. S10A**). Further additions of NaOH determined an initial blue shift at 345 nm followed by a red shift at 394 nm (see **Fig. S10B**, pH 5.57). In the pH range 5.57 - pH 10.82 a slight increase of absorbance was observed (**Fig. S10B**).

Spectral variations observed during the titration of 3

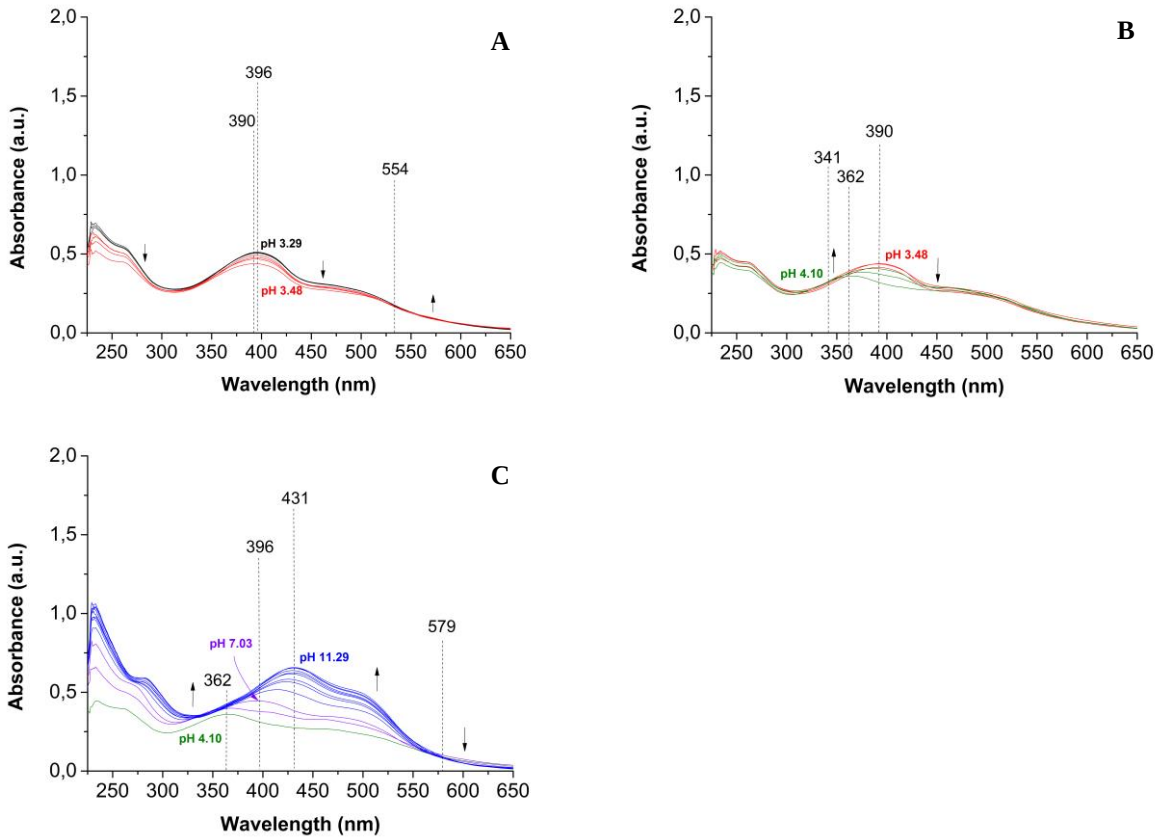

Fig. S11. Selected spectra collected during the potentiometric and spectrophotometric titration of **3** (1.30×10^{-4} M, 0.1 M NaCl, *t* 25°C, optic path length 0.5 cm) from pH 3.29 to 3.48 (**A**); from pH 3.48 to 4.10 (**B**); from pH 4.10 to 11.29 (**C**).

presence of five equilibria. The first spectrum (pH 3.29) shown a peak at 396 nm with a shoulder at 473 nm, and after the firsts NaOH additions, a decrease in terms of absorbance and a slight blue shift at 390 nm together with the formation of an isosbestic point at 554 nm were observed (**Fig. S11A**). Further increases of titrant determined a change of the spectral profile, with the formation of a band at 362 nm and an isosbestic point at 341 nm (**Fig. S11B**). In the pH range 4.10 - 7.03 a red shift towards 396 nm and an increase in absorbance were observed. In the same pH range the solution appeared slightly turbid. With higher NaOH additions, a gradual shift towards wavelengths 431 nm with an increase in absorbance and the formation of an isosbestic point at 597 nm were observed. In this pH range the turbidity previously mentioned completely disappeared (**Fig. S11C**).

Spectral variations observed during the titration of 4

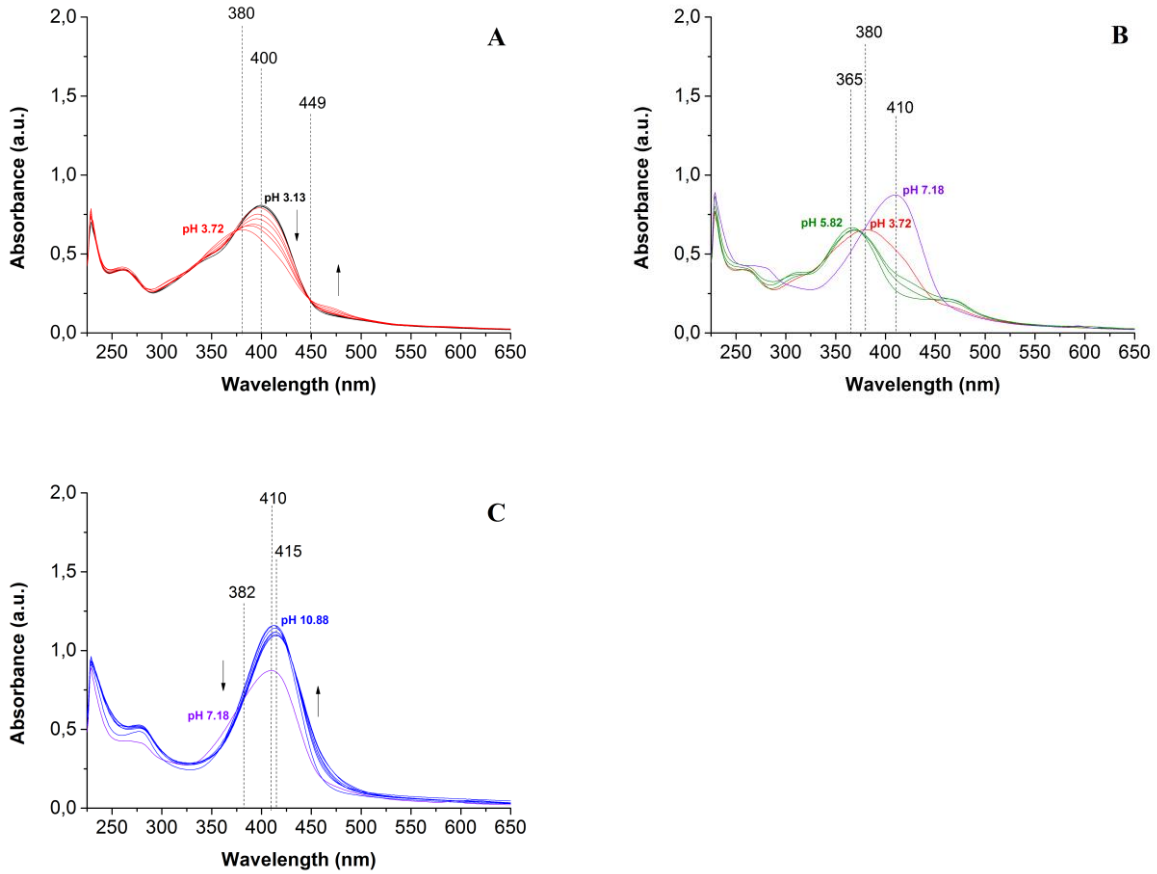

Fig. S12. Selected spectra collected during the potentiometric and spectrophotometric titration of **4** (1.25×10^{-4} M, 0.1 M NaCl, *t* 25°C, optic path length 0.5 cm) from pH 3.13 to 3.72 (**A**); from pH 3.72 to 7.18 (**B**); from pH 7.18 to 10.88 (**C**).

Five chemical equilibria were identified from the analysis of the spectra recorded during the titration of **4** (pH range 3.13-10.88). The first spectrum (pH 3.13) shown a peak at 400 nm, while after the first additions of NaOH, a decrease in terms of absorbance, accompanied by a slight blue shift at 380 nm and the formation of an isosbestic point at 449 nm were observed (**Fig. S12A**). In the pH range 3.72 - 5.82, a band at 365 nm and at pH 7.18 a peak at 410 nm appeared (**Fig. S12B**). In the same pH range the solution was slightly turbid. With further NaOH additions, a gradual shift towards higher wavelengths (415 nm), with an increase of the absorbance and an isosbestic point at 382 nm were observed. In this pH range the turbidity previously mentioned completely disappeared (**Fig. S12C**).

Spectral variations observed during the titration of 5

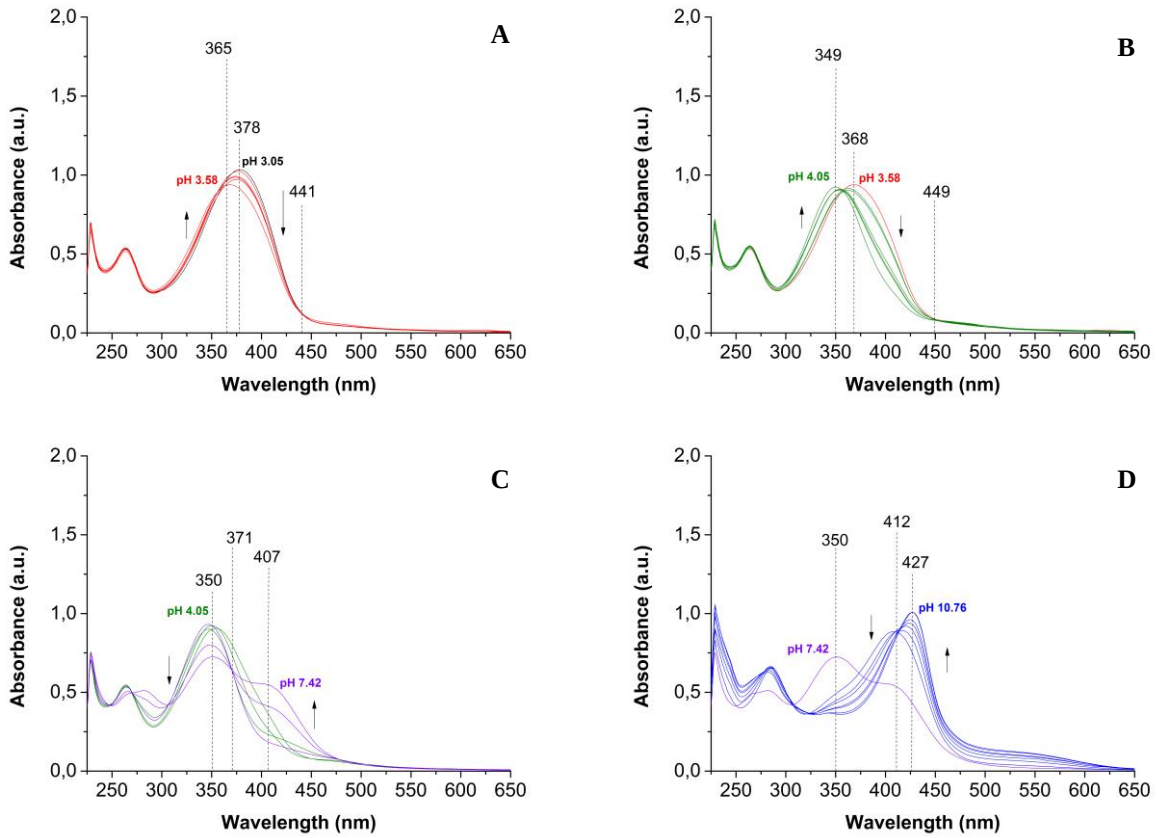

Fig. S13. Selected spectra collected during the potentiometric and spectrophotometric titration of **5** (1.24×10^{-4} M, 0.1 M NaCl, *t* 25°C, optic path length 0.5 cm) from pH 3.05 to 3.58 (**A**); from pH 3.58 to 4.05 (**B**); from pH 4.05 to 7.42(**C**); from pH 7.42 to 10.76 (**D**).

The inspection of the spectra recorded during the titration of **5** (pH range 3.05-10.76) evidenced the presence of five equilibria. The first spectrum (pH 3.05) shown a peak at 378 nm, while after the firsts additions of titrant (pH range 3.05-3.58), a decrease in terms of absorbance and a blue shift at 365 nm together with the formation of an isosbestic point at 441 nm were observed (**Fig. S13A**). Further additions of NaOH (pH 3.58-4.05) determined a change of the spectral profile, with the formation of a new band at 349 nm and an isosbestic point at 449 nm (**Fig. S13B**). In the pH range 4.05 - 7.42 an additional decrease in absorbance with the formation of an overlapped peak at 407 nm and an isosbestic point at 371 nm were also observed (**Fig. S13C**). Further additions of NaOH

(pH range 7.42-10.76), determined a progressive shift towards higher wavelengths (427 nm) and an increase in absorbance and the formation of an isosbestic point at 412 nm (**Fig. S13D**).

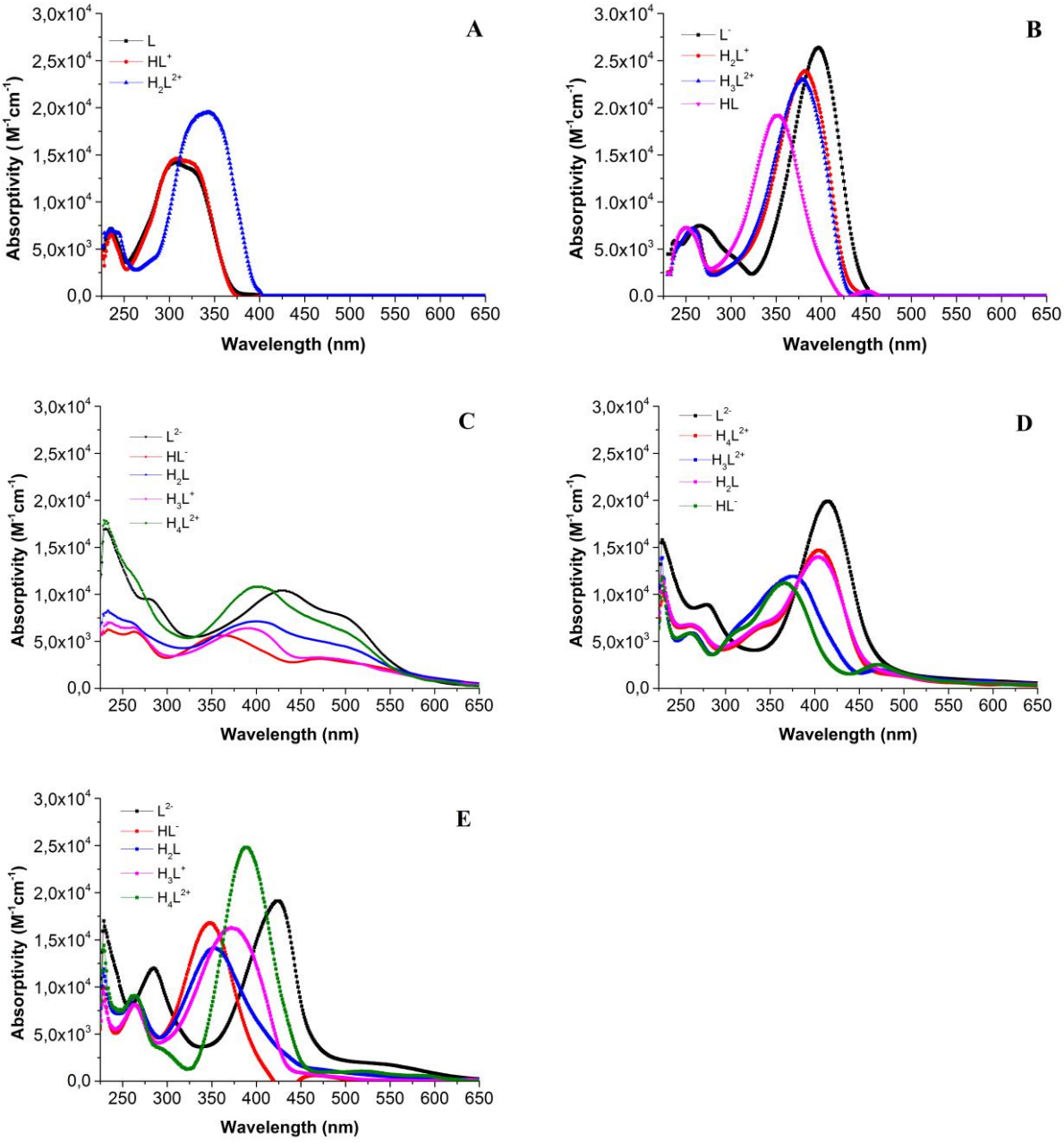

Fig. S14. Calculated pure spectra obtained from the eigenvalue analyses of potentiometric and spectrophotometric titrations of **1-5** (**A-E**).

3. Antioxidant tests

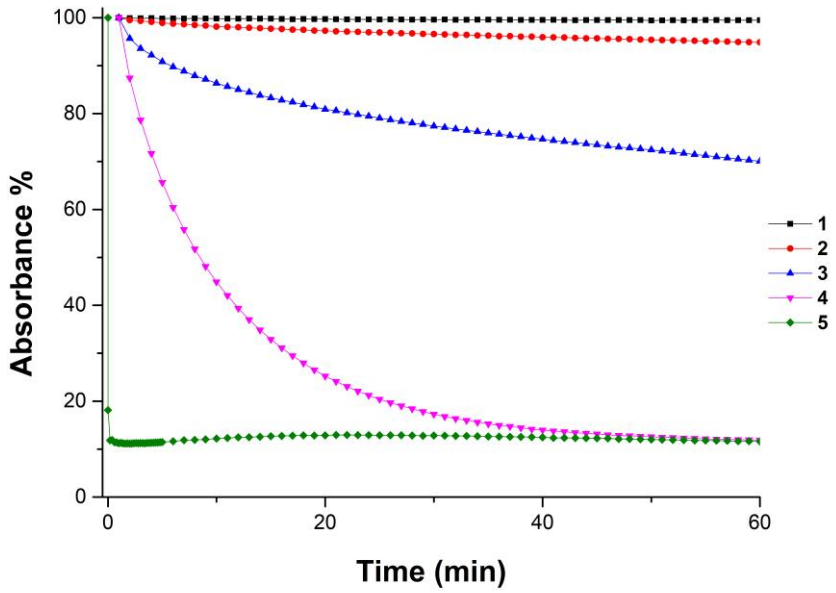

Fig. S15. Reducing activity of DPP· shown by the studied compounds (0.05 mM, absolute ethanol, *t* 25 °C, λ 517 nm).

4. Soybean lipoxygenase inhibition tests

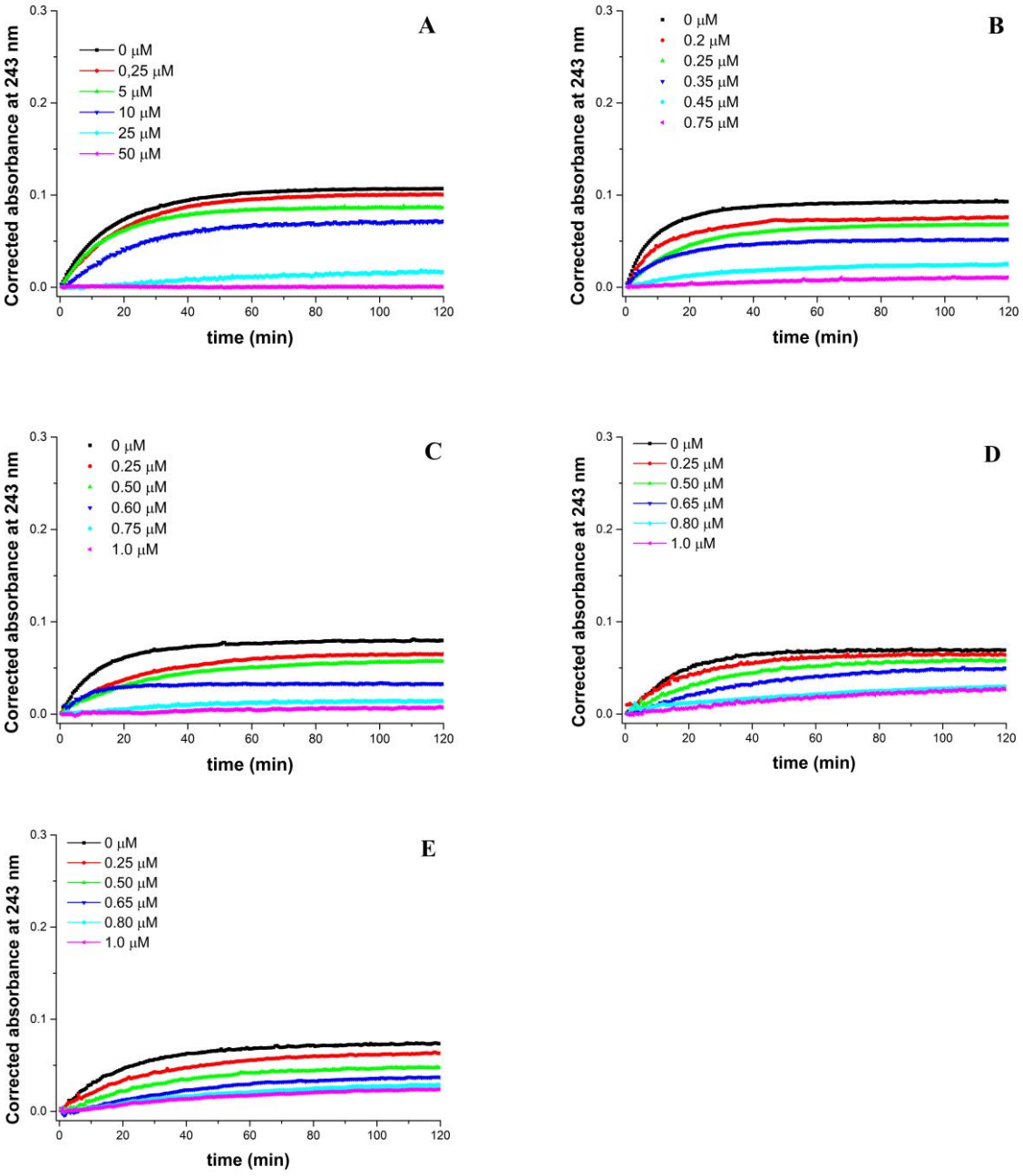

Fig. S16. Absorbance at 243 nm of solutions containing sodium linoleate, lipoxygenase enzyme and **1-5** (**A-E**) at different molar concentration. Sodium linoleate 14 μM, lipoxygenase 0.83 nM, pH 7.4 TRIS buffer, *t* 25°C. Values are corrected for absorbance of ligands.

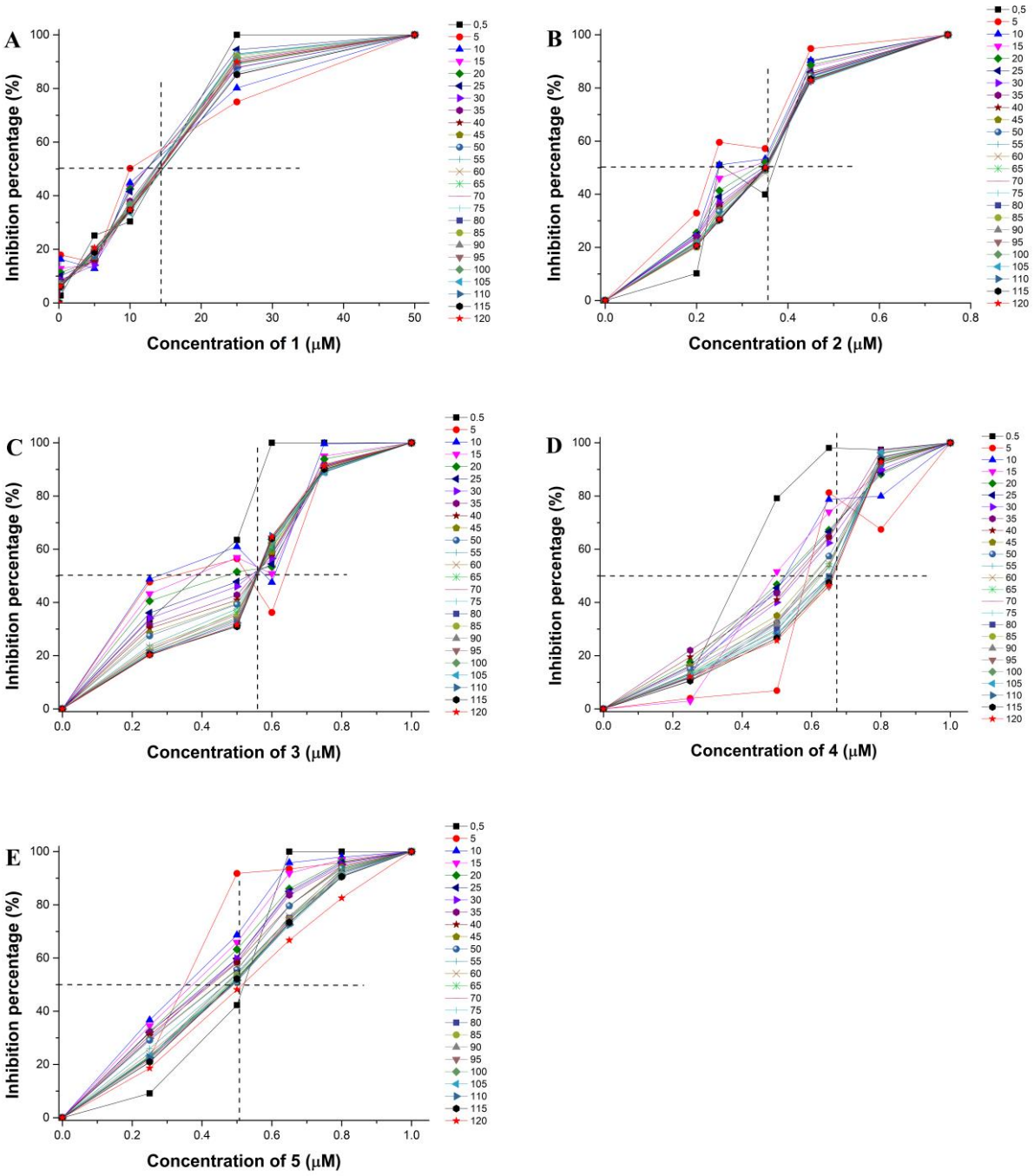

Fig. S17 Inhibition percentages (IP%) observed at different concentrations of solutions containing sodium linoleate, lipoxygenase enzyme and **1**-**5** (**A**-**E**). Sodium linoleate 14 μM, lipoxygenase 0.83 nM, pH 7.4 TRIS buffer, *t* 25°C.

5. Computational details

HAT, SETPT and SPLET description

The Hydrogen Atom Transfer (**HAT**), the Single Electron Transfer Proton Transfer (**SETPT**) and the Sequential Proton Loss Electron Transfer (**SPLET**) mechanisms, commonly adopted by antioxidant phenolics are briefly explained:

1. Hydrogen Atom Transfer (**HAT**), where a radical hydrogen is directly abstracted from the phenolic antioxidant (**R1**). The Bond Dissociation Enthalpy (**BDE, eq.1**) quantitatively describes this reaction path.

   $ArOH \rightarrow ArO^{\cdot} + H^{\cdot}$ $(\boldsymbol{R1})$ $\qquad$ $\boldsymbol{BDE} = H(ArO^{\cdot}) + H(H^{\cdot}) - H(ArOH)$ $(\boldsymbol{eq.1})$

2. Single Electron Transfer Proton Transfer (**SETPT**), where the extraction of an electron from the antioxidant (**R2a**) is followed by proton removal from the subsequent radical cation (**R2b**). Ionization Potential (**IP, eq.2a**) and Proton Dissociation Enthalpy (**PDE, eq.2b**) are commonly exploited to describe the two steps, respectively. The thermochemical parameter **SETPT** (**eq.2**) considers the process in its entirety.

   $ArOH \rightarrow ArOH^{+\cdot} + e^{-}$ $(\boldsymbol{R2a})$ $\qquad$ $\boldsymbol{IP} = H(ArOH^{+\cdot}) + H(e^{-}) - H(ArOH)$ $(\boldsymbol{eq.2a})$

   $ArOH^{+\cdot} \rightarrow ArO^{\cdot} + H^{+}$ $(\boldsymbol{R2b})$ $\qquad$ $\boldsymbol{PDE} = H(ArO^{\cdot}) + H(H^{+}) - H(ArOH^{+\cdot})$ $(\boldsymbol{eq.2b})$

   $\boldsymbol{SETPT} = \boldsymbol{IP} + \boldsymbol{PDE}$ $(\boldsymbol{eq.2})$

3. Sequential Proton Loss Electron Transfer (**SPLET**), where the phenolic antioxidant is firstly deprotonated (**R3a**) then converted in its neutral radical by single electron transfer (**R3b**). The first step is described by the Proton Affinity (**PA, eq.3a**), while the second one is

quantitatively defined by the Electron Transfer Enthalpy (**ETE, eq.3b**). The thermochemical parameter **SPLET** (**eq.3**) contemplates the process in its entirety.

$ArOH \rightarrow ArO^- + H^+$ $(\boldsymbol{R3a})$ $\qquad \boldsymbol{PA} = H(ArO^-) + H(H^+) - H(ArOH)$ $(\boldsymbol{eq.3a})$

$ArO^- \rightarrow ArO^{\cdot} + e^-$ $(\boldsymbol{R3b})$ $\qquad \boldsymbol{ETE} = H(ArO^{\cdot}) + H(e^-) - H(ArO^-)$ $(\boldsymbol{eq.3a})$

$\boldsymbol{SPLET} = \boldsymbol{PA} + \boldsymbol{ETE}$ $(\boldsymbol{eq.3})$

Chemical formalisms and equations used for the calculation of the enthalpies.

$H^+_{(gas)} + H_2O_{(aq)} \rightarrow H_3O^+_{(aq)}$

$\boldsymbol{H\left[H^+_{(aq)}\right] = H\left[H_3O^+_{(aq)}\right] - H\left[H_2O_{(aq)}\right] - H\left[H^+_{(gas)}\right]}$

$H_2O_{(aq)} + e^-_{(gas)} \rightarrow H_2O^{-\cdot}_{(aq)}$

$\boldsymbol{H\left[e^-_{(aq)}\right] = H\left[H_2O^{-\cdot}_{(aq)}\right] - H\left[H_2O_{(aq)}\right] - H\left[e^-_{(gas)}\right]}$

$H^+_{(gas)} + CH_3CH_2OH_{(solv)} \rightarrow CH_3CH_2OH_2^+{}_{(solv)}$

$\boldsymbol{H\left[H^+_{(solv)}\right] = H\left[CH_3CH_2OH_2^+{}_{(solv)}\right] - H\left[CH_3CH_2OH_{(solv)}\right] - H\left[H^+_{(gas)}\right]}$

$CH_3CH_2OH_{(solv)} + e^-_{(gas)} \rightarrow CH_3CH_2OH^{-\cdot}_{(solv)}$

$\boldsymbol{H\left[e^-_{(solv)}\right] = H\left[CH_3CH_2OH^{-\cdot}_{(solv)}\right] - H\left[CH_3CH_2OH_{(solv)}\right] - H\left[e^-_{(gas)}\right]}$

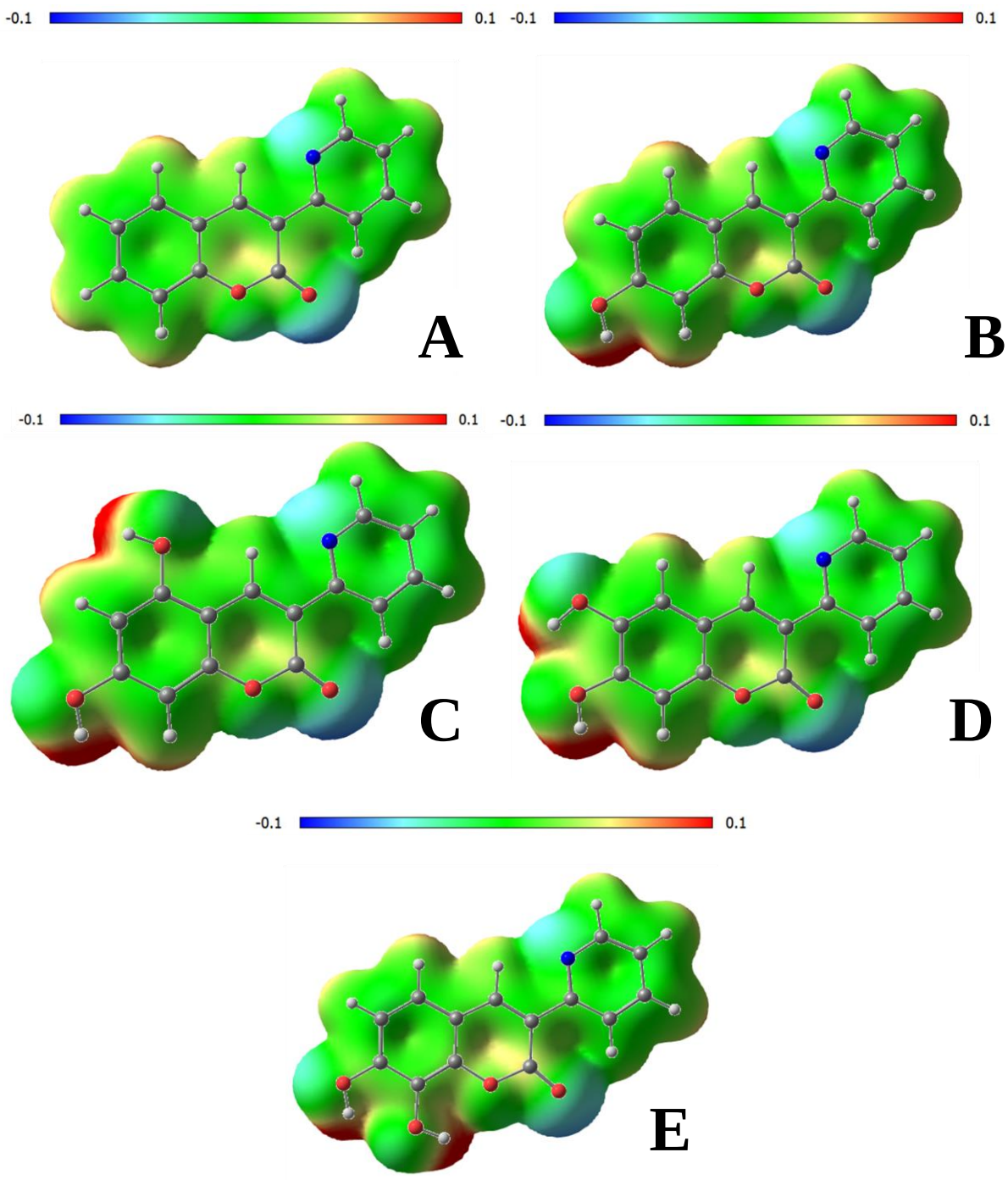

Fig. S18. Electrostatic Potential Maps (contour plot: 0.005) for **1-5** (**A-E**) at the DFT-optimized geometries (gas phase).

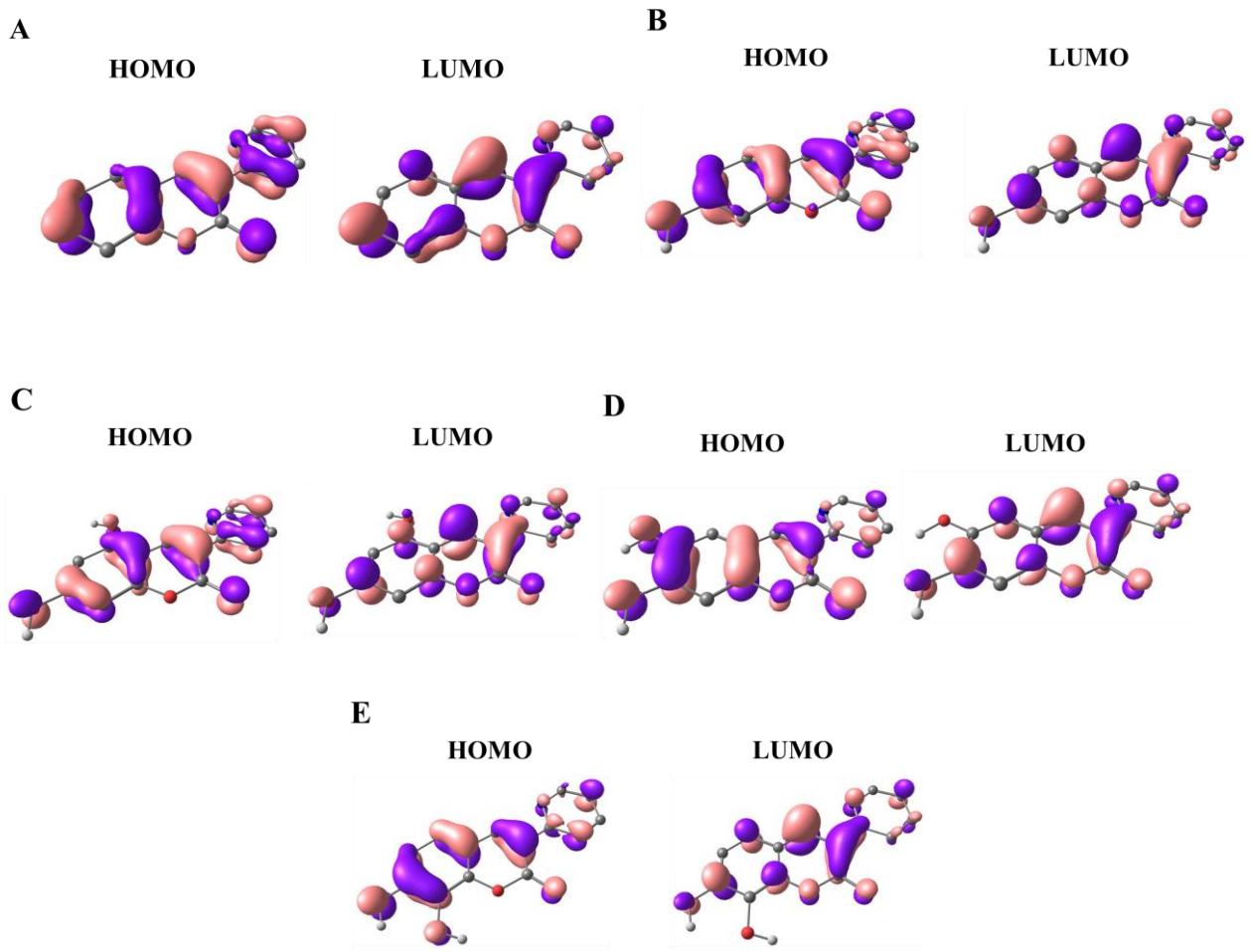

Fig. S19 Gas-phase frontier Molecular Orbitals plots (contour value: 0.005) of **1-5** (**A-E**).

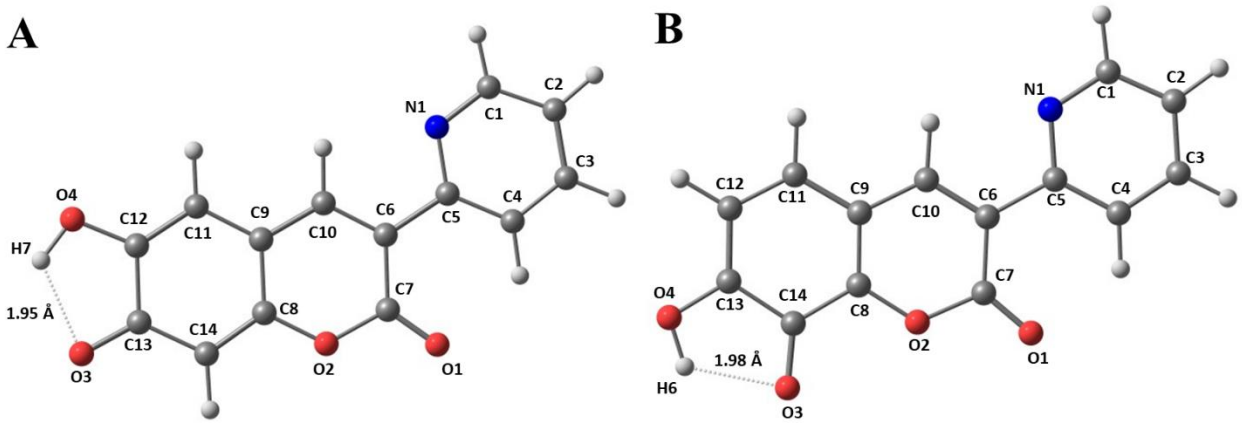

Fig. S20. Molecular drawings and atom labelling scheme for the most stable radical species of **4** (**A**) and **5** (**B**) at the DFT-optimized geometries (gas phase).

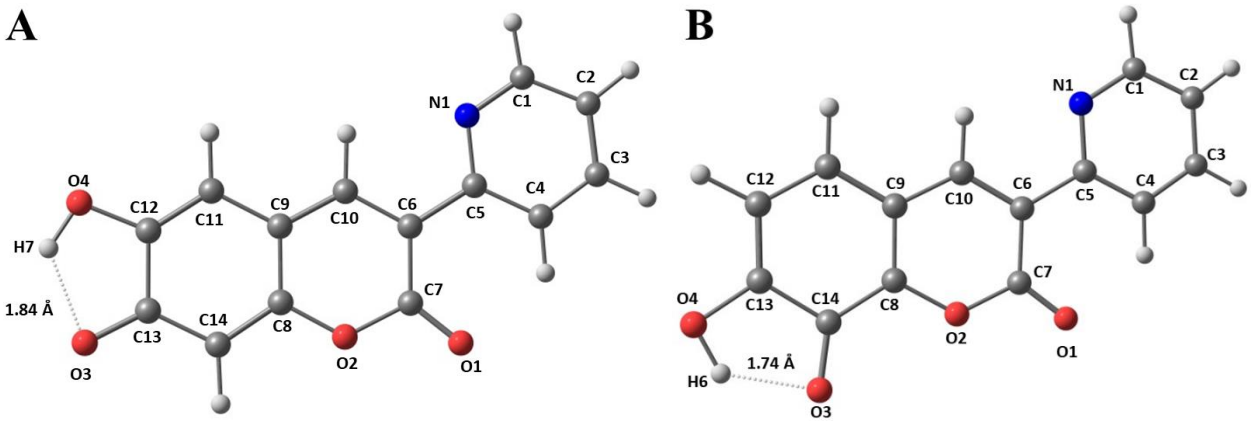

Fig. S21. Molecular drawings and atom labelling scheme for the most stable monoanionic species of **4** (**A**) and **5** (**B**) at the DFT-optimized geometries (gas phase).

A

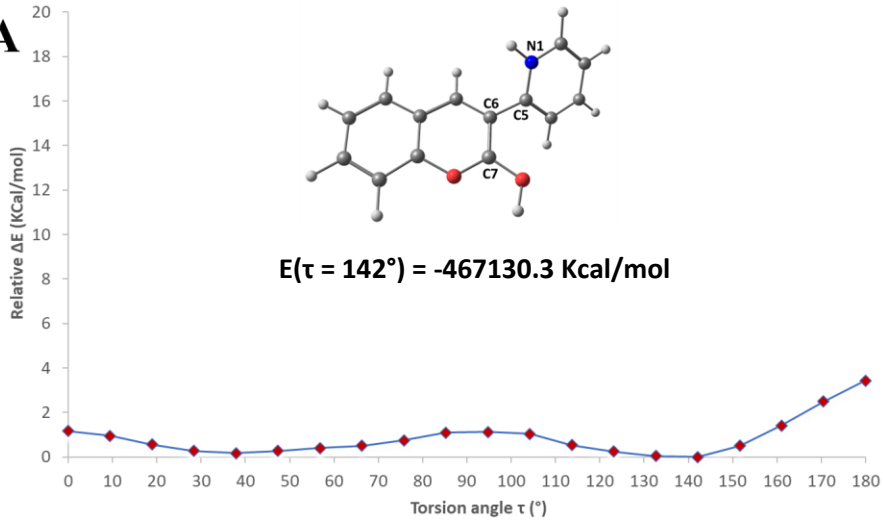

E(τ = 142°) = -467130.3 Kcal/mol

B

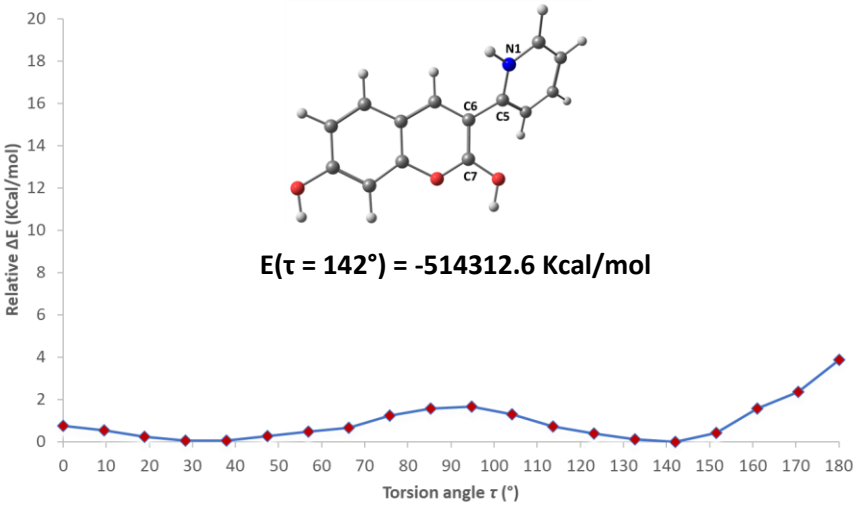

E(τ = 142°) = -514312.6 Kcal/mol

C

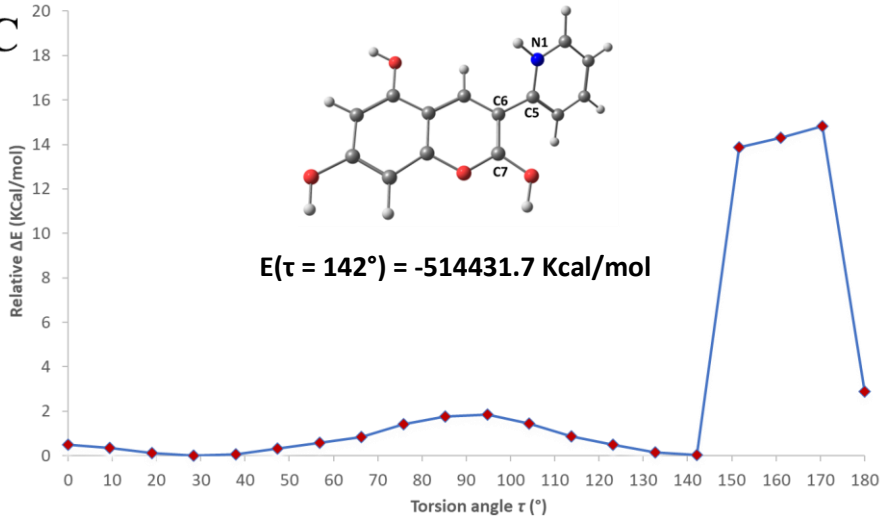

E(τ = 142°) = -514431.7 Kcal/mol

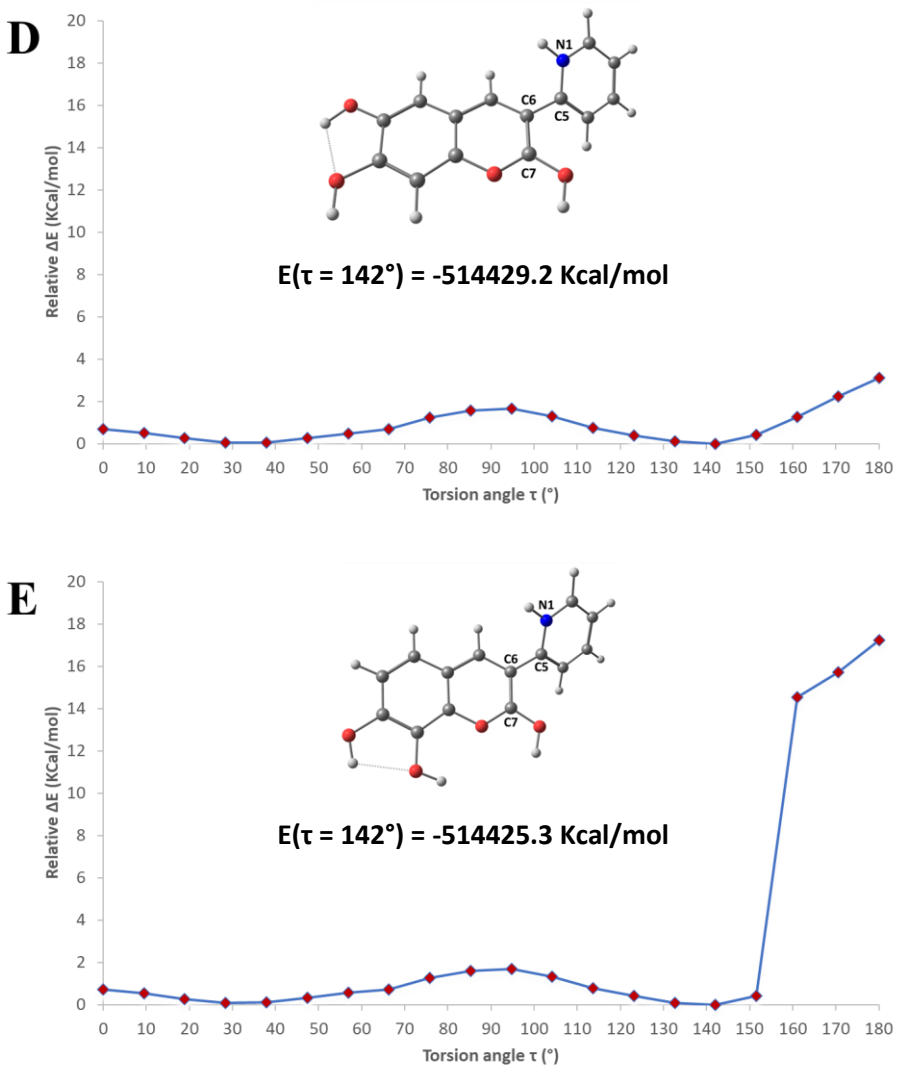

Fig. S22. Relative variation ΔE of the total electronic energy as a function of torsion angle τ (C7–C6–C5–N1 dihedral) calculated for the bis-cationic species of Gas-phase frontier Molecular Orbitals plots (contour value: 0.005) of **1-5** (**A-E**) at the DFT level (PBE0, def-2 TZVP) in water (CPCM).

A

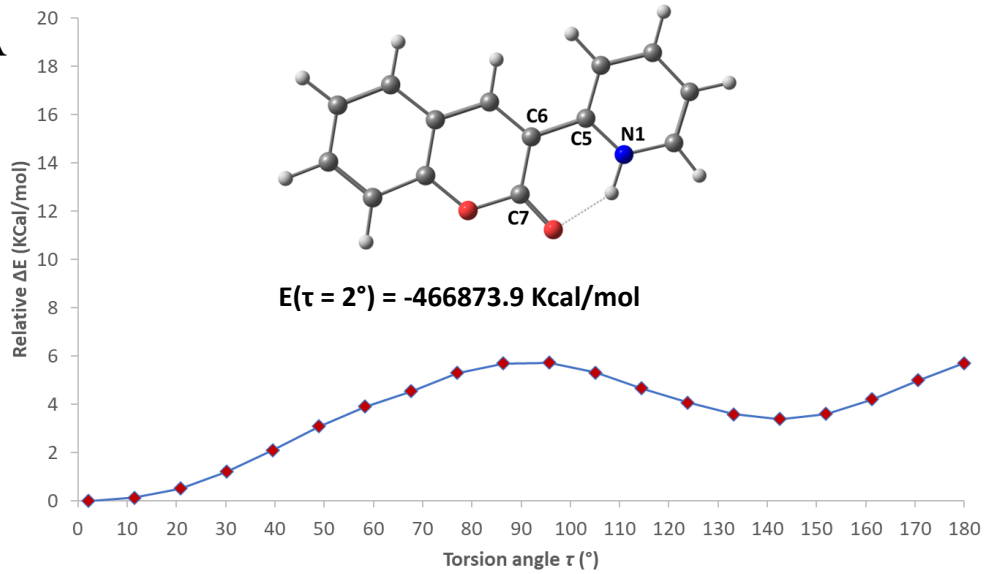
C6
C5
N1
C7
E(τ = 2°) = -466873.9 Kcal/mol
Relative ΔE (KCal/mol)
Torsion angle τ (°)

B

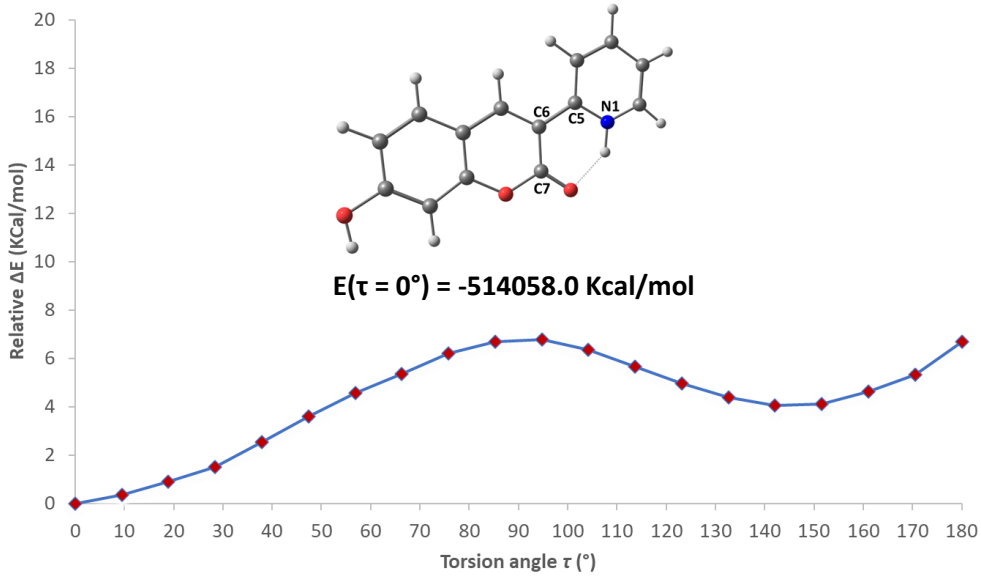
C6
C5
N1
C7
E(τ = 0°) = -514058.0 Kcal/mol
Relative ΔE (KCal/mol)
Torsion angle τ (°)

C

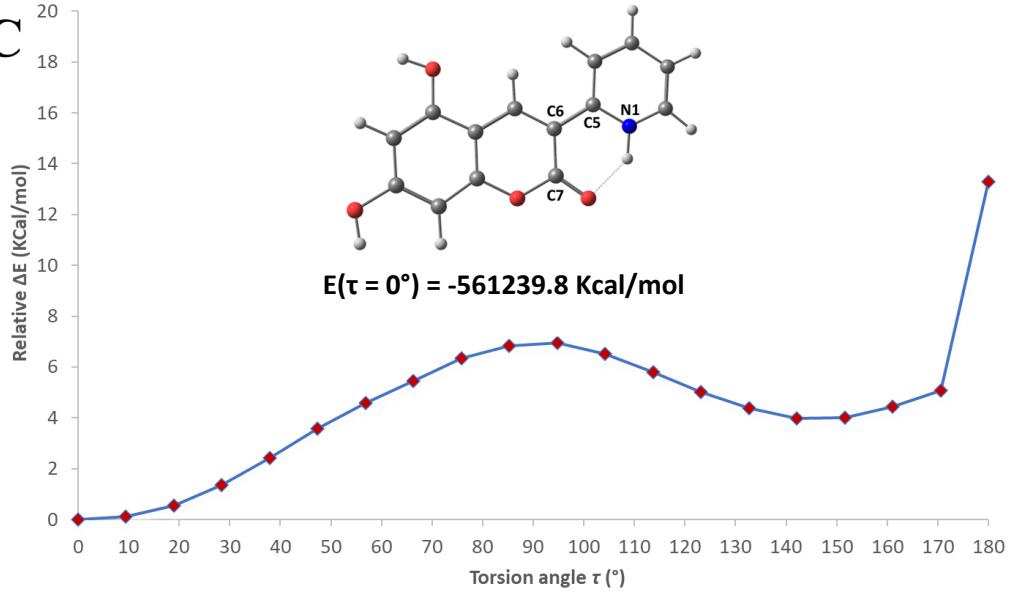
C6
C5
N1
C7
E(τ = 0°) = -561239.8 Kcal/mol
Relative ΔE (KCal/mol)
Torsion angle τ (°)

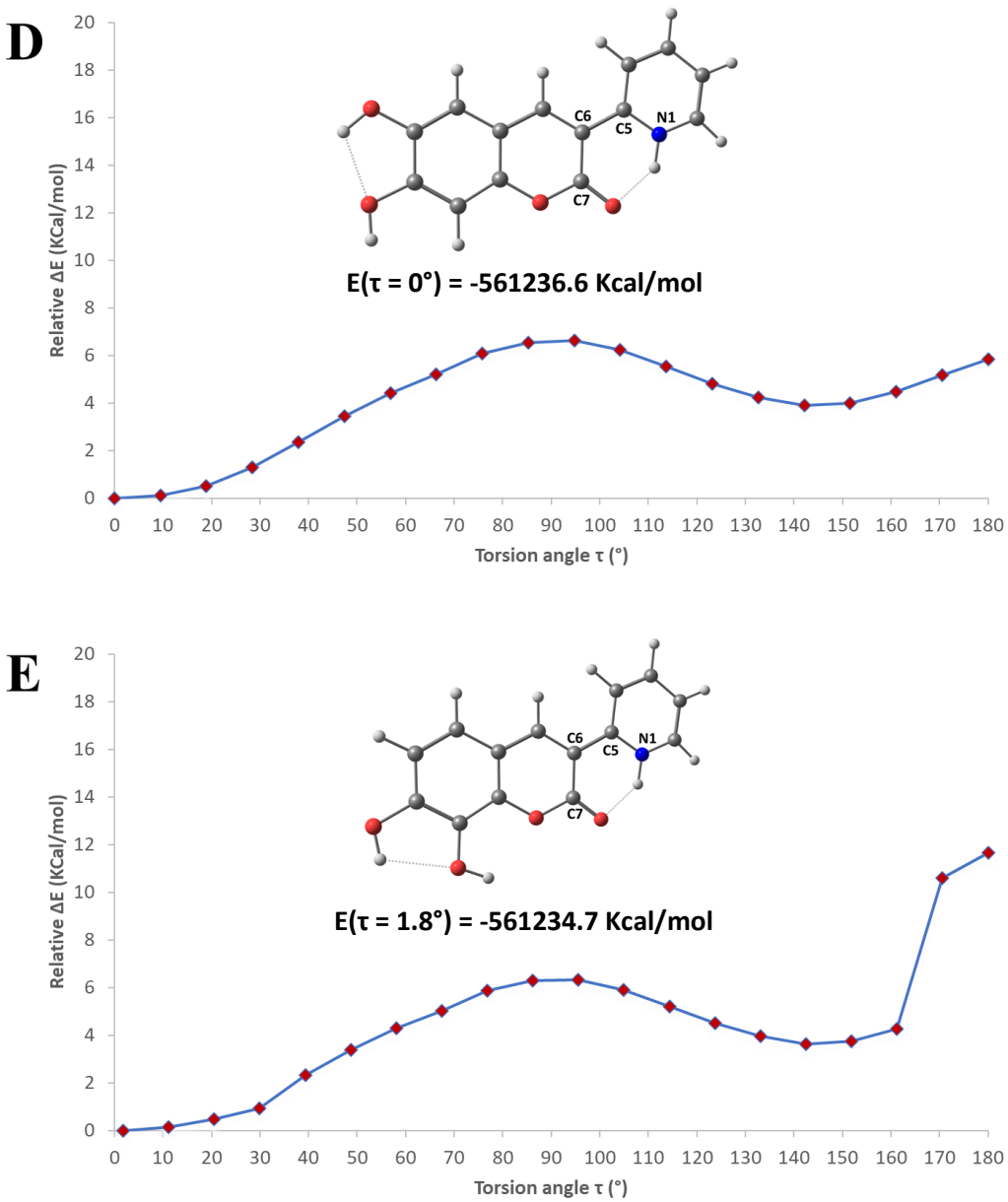

Fig. S23. Relative variation ΔE of the total electronic energy as a function of torsion angle τ (C7–C6–C5–N1 dihedral) calculated for the mono-cationic species of **1-5** (**A-E**) at the DFT level (PBE0, def-2 TZVP) in water (CPCM).

A

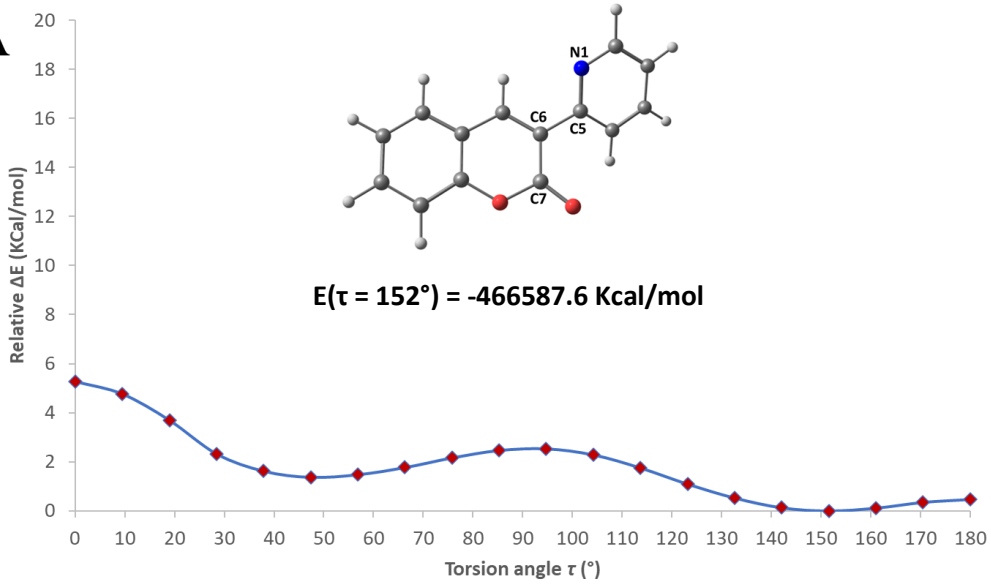
N1
C6
C5
C7
E(τ = 152°) = -466587.6 Kcal/mol
Relative ΔE (KCal/mol)
Torsion angle τ (°)

B

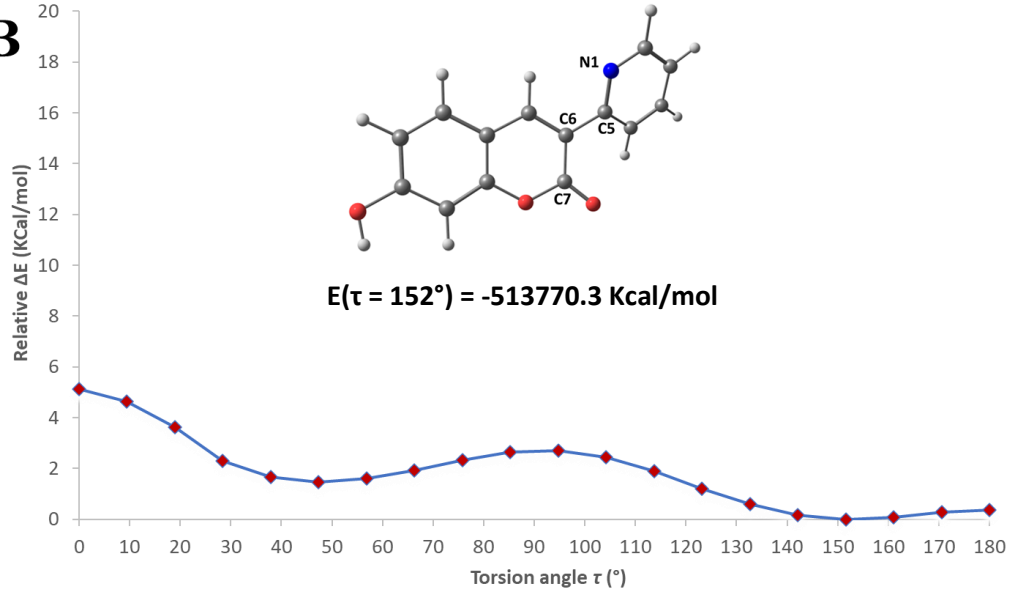
N1
C6
C5
C7
E(τ = 152°) = -513770.3 Kcal/mol
Relative ΔE (KCal/mol)
Torsion angle τ (°)

C

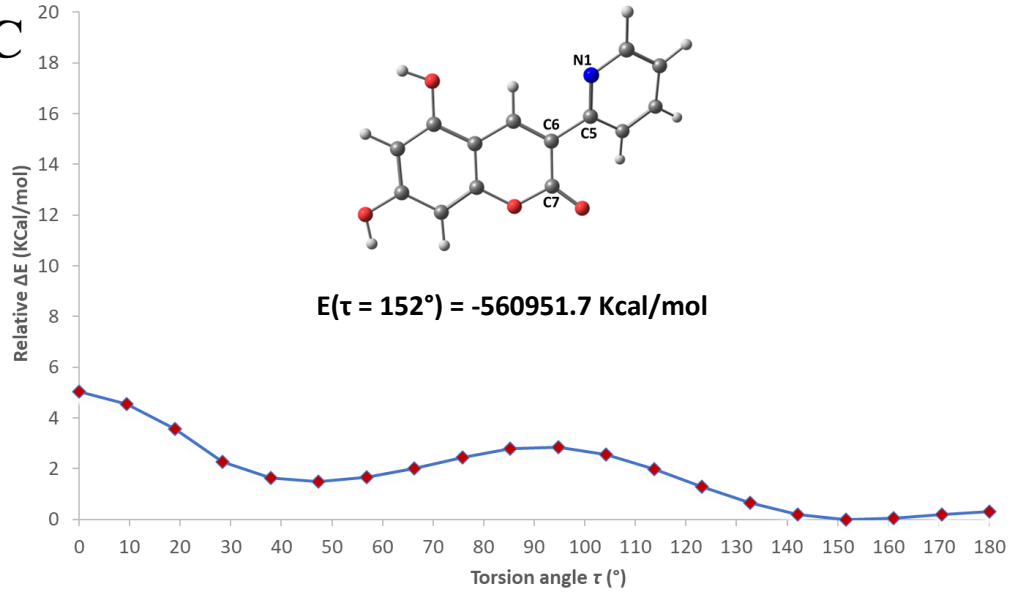
N1
C6
C5
C7
E(τ = 152°) = -560951.7 Kcal/mol
Relative ΔE (KCal/mol)
Torsion angle τ (°)

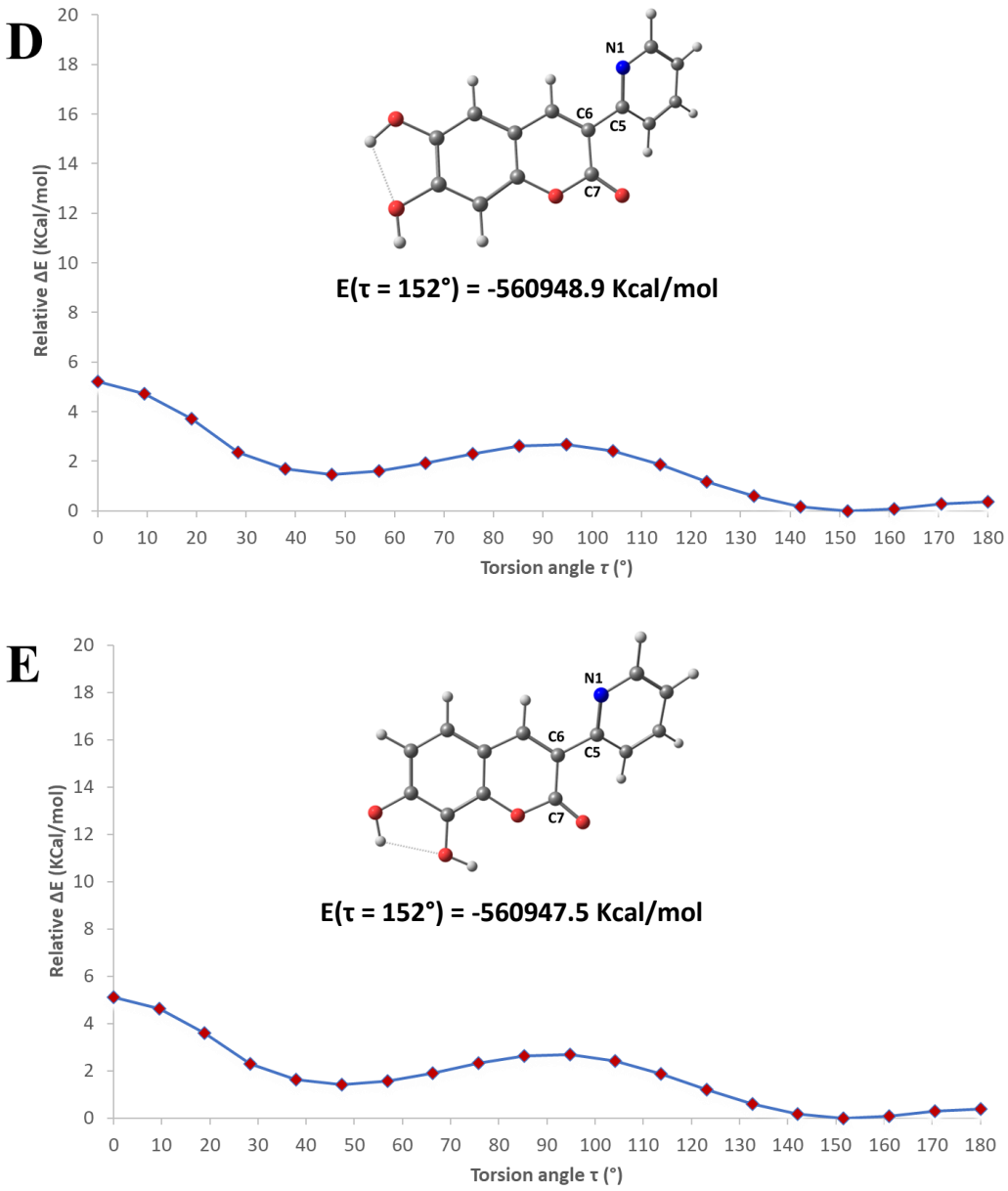

Fig. S24. Relative variation ΔE of the total electronic energy as a function of torsion angle τ (C7–C6–C5–N1 dihedral) calculated for **1-5** (**A-E**) at the DFT level (PBE0, def-2 TZVP) in water (CPCM).

A

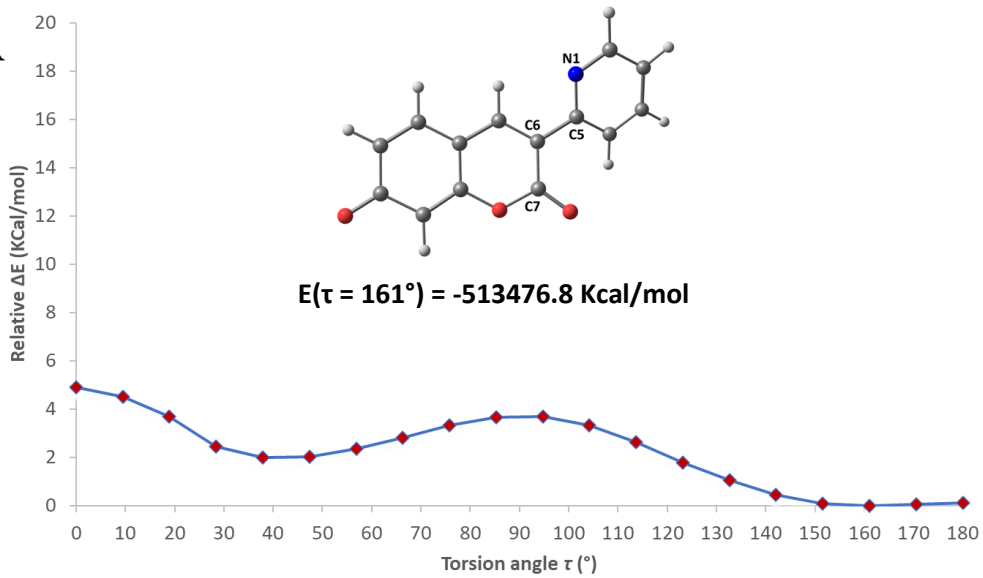
N1
C6
C5
C7
E(τ = 161°) = -513476.8 Kcal/mol
Relative ΔE (KCal/mol)
Torsion angle τ (°)

B

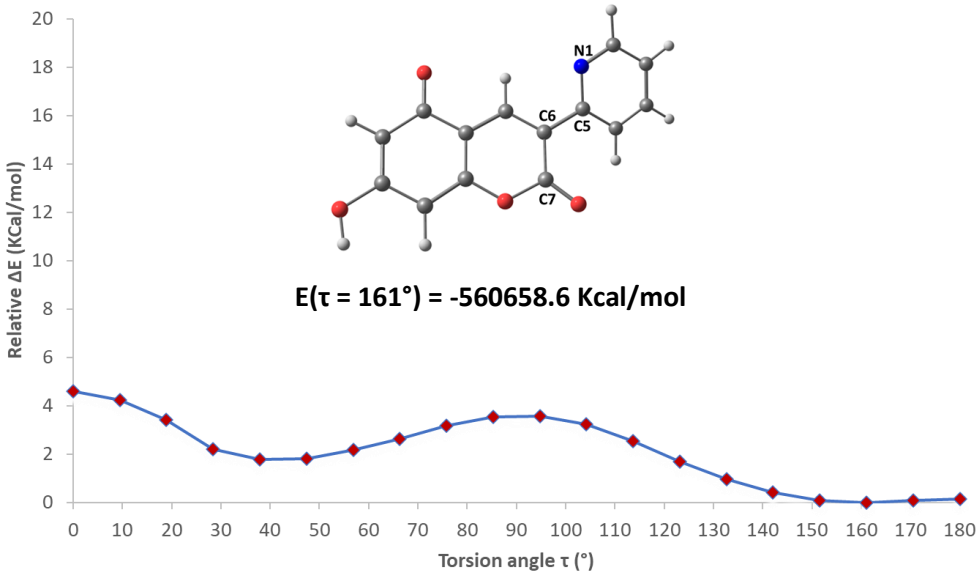
N1
C6
C5
C7
E(τ = 161°) = -560658.6 Kcal/mol
Relative ΔE (KCal/mol)
Torsion angle τ (°)

C

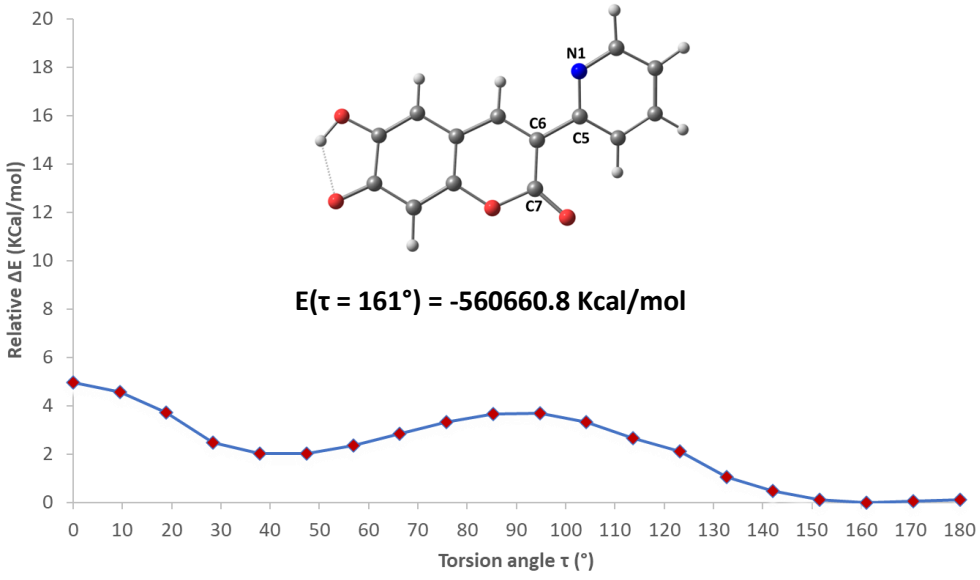
N1
C6
C5
C7
E(τ = 161°) = -560660.8 Kcal/mol
Relative ΔE (KCal/mol)
Torsion angle τ (°)

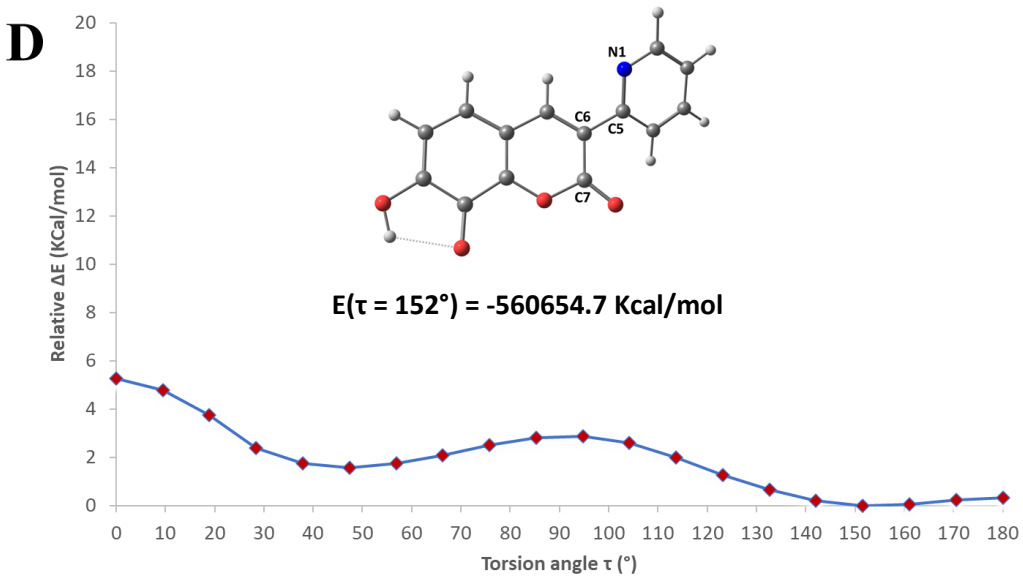

Fig. S25. Relative variation ΔE of the total electronic energy as a function of torsion angle τ (C7–C6–C5–N1 dihedral) calculated for the monoanionic species of **2** (**A**), **3** (**B**), **4** (**C**) and **5** (**D**) at the DFT level (PBE0, def-2 TZVP) in water (CPCM).

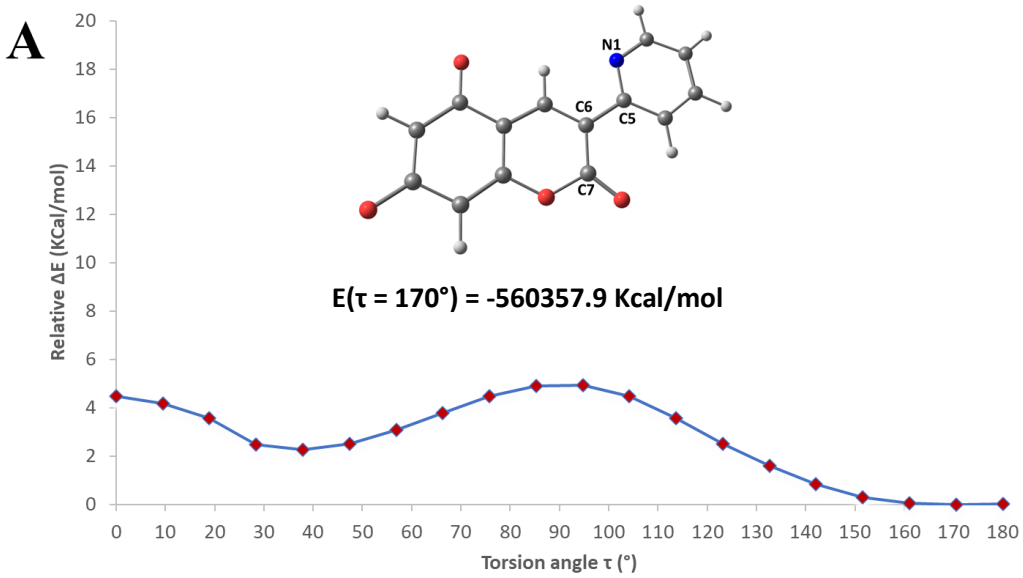

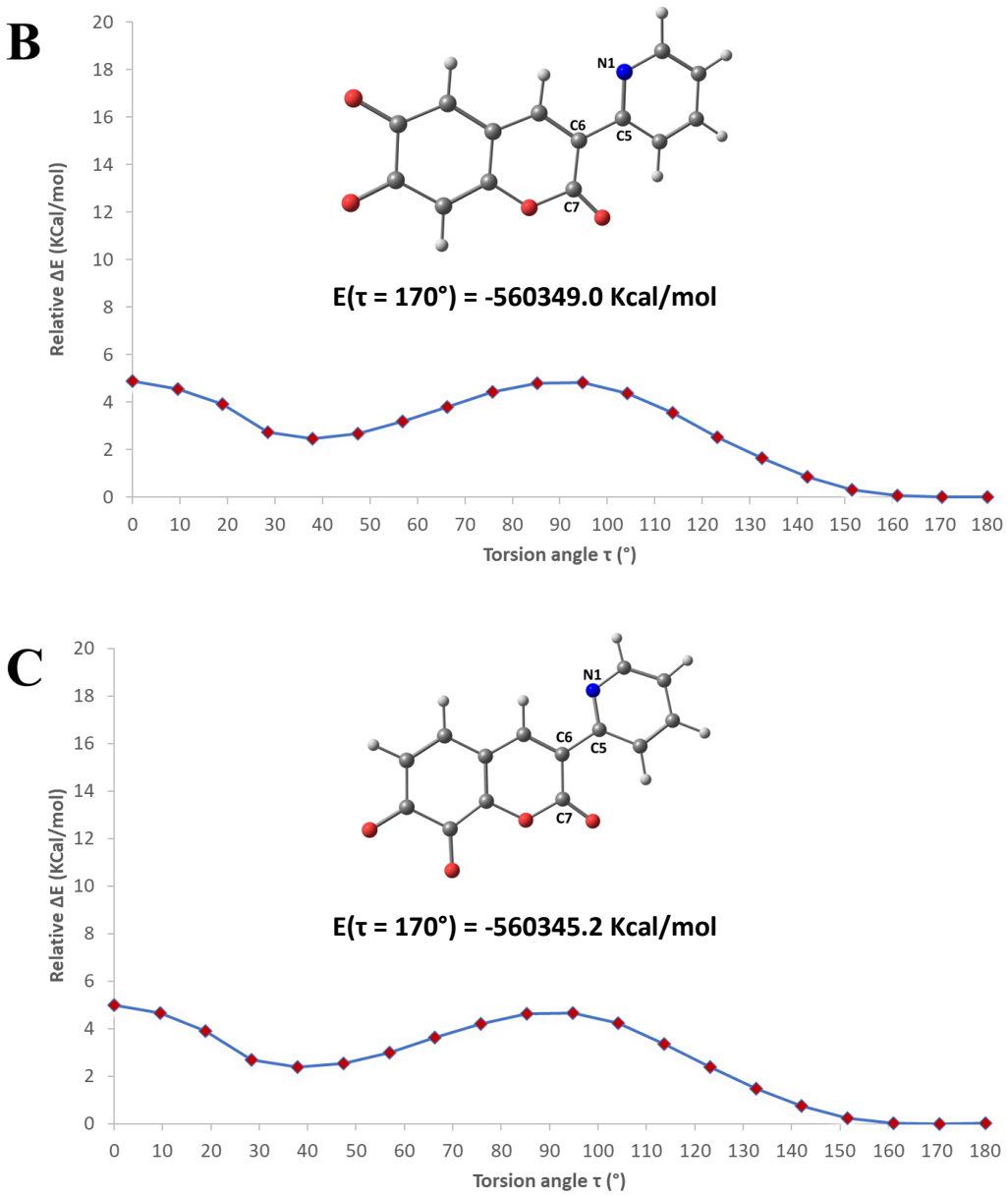

Fig. S26. Relative variation ΔE of the total electronic energy as a function of torsion angle τ (C7–C6–C5–N1 dihedral) calculated for the bis-cationic species of **3** (**A**), **4** (**B**) and **5** (**C**) at the DFT level (PBE0, def-2 TZVP) in water (CPCM).

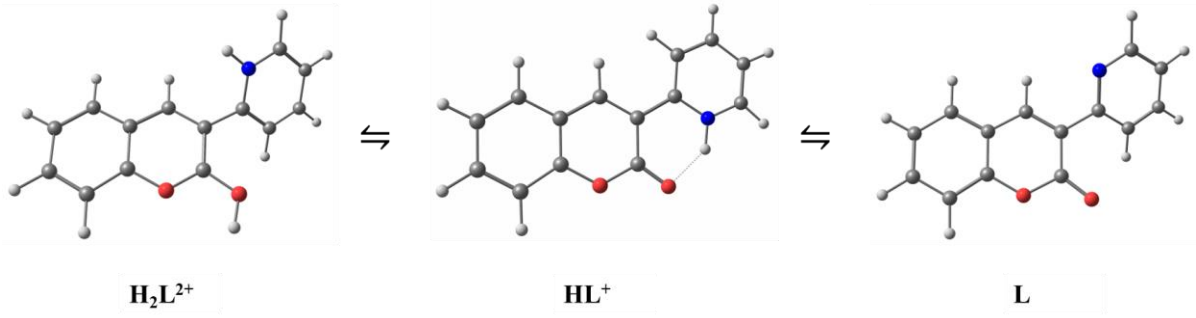

Fig. S27. Protonation sequence proposed for compound **1** based on experimental (potentiometric and spectrophotometric titrations) and theoretical data (DFT-PBE0/def-2 TZVP, water CPCM). The lowest-energy conformer for each differently protonated species is reported.

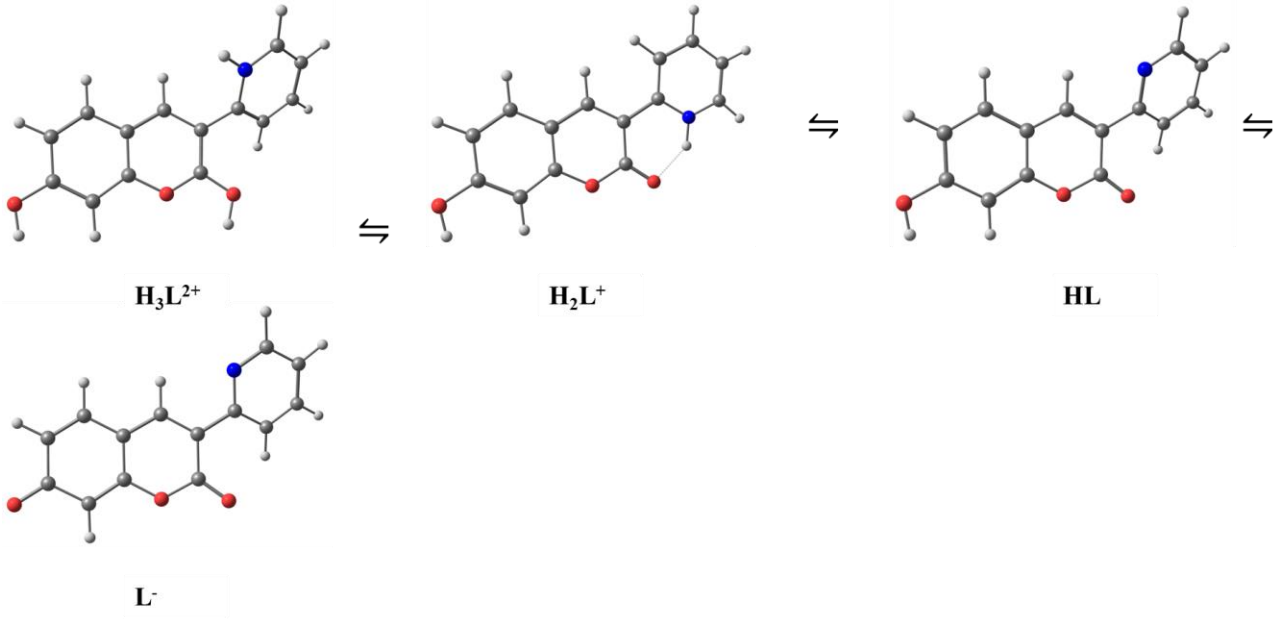

Fig. S28. Protonation sequence proposed for compound **2** based on experimental (potentiometric and spectrophotometric titrations) and theoretical data (DFT-PBE0/def-2 TZVP, water CPCM). The lowest-energy conformer for each differently protonated species is reported.

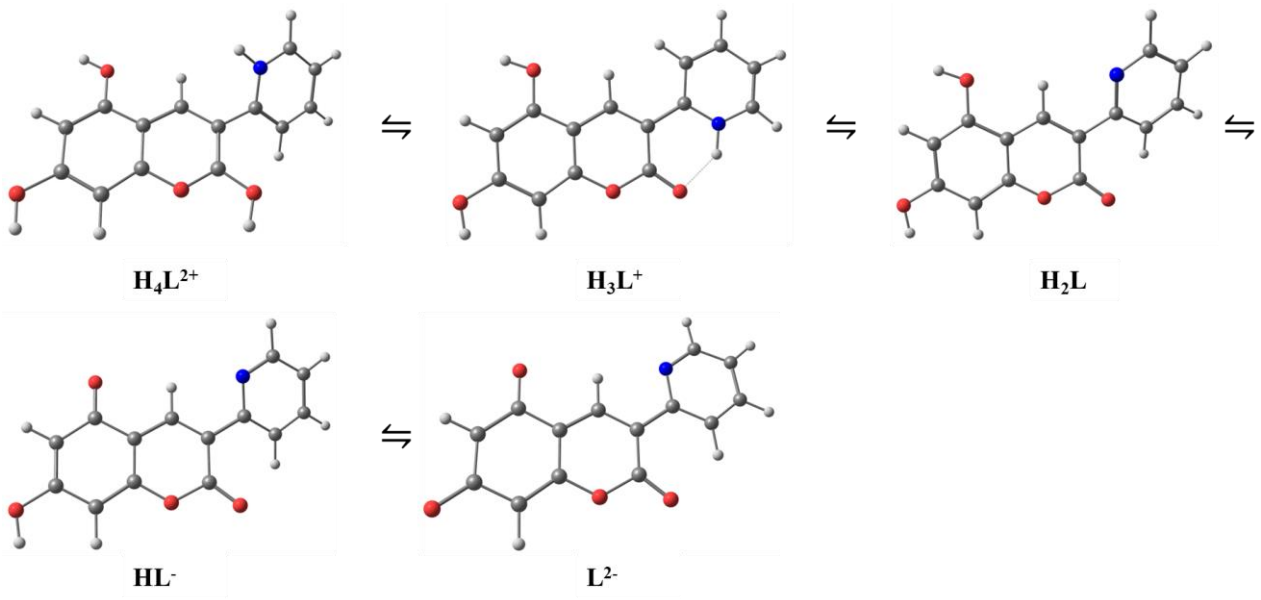

Fig. S29. Protonation sequence proposed for compound **3** based on experimental (potentiometric and spectrophotometric titrations) and theoretical data (DFT-PBE0/def-2 TZVP, water CPCM). The lowest-energy conformer for each differently protonated species is reported.

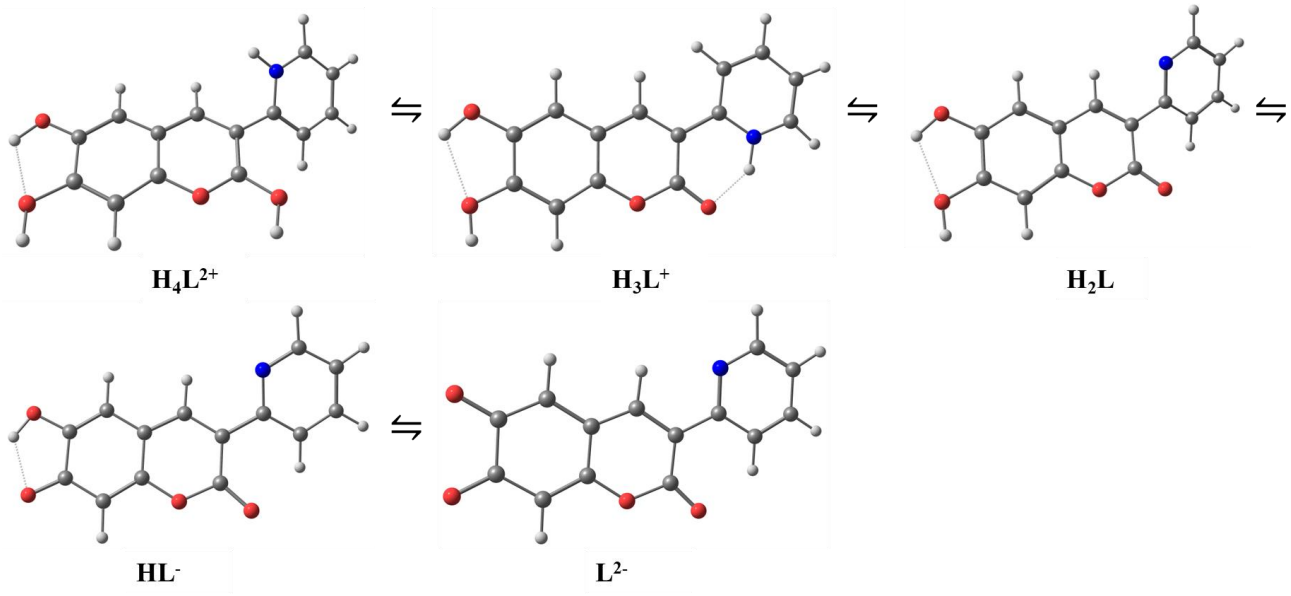

Fig. S30. Protonation sequence proposed for compound **4** based on experimental (potentiometric and spectrophotometric titrations) and theoretical data (DFT-PBE0/def-2 TZVP, water CPCM). The lowest-energy conformer for each differently protonated species is reported.

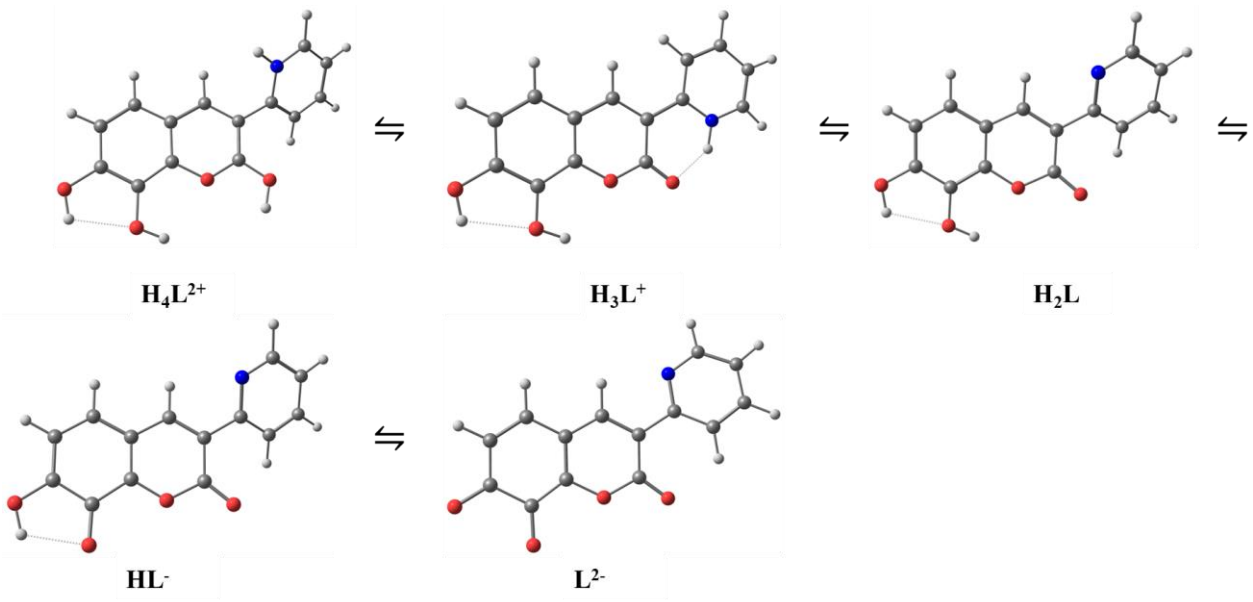

Fig. S31. Protonation sequence proposed for compound **5** based on experimental (potentiometric and spectrophotometric titrations) and theoretical data (DFT-PBE0/def-2 TZVP, water CPCM). The lowest-energy conformer for each differently protonated species is reported.

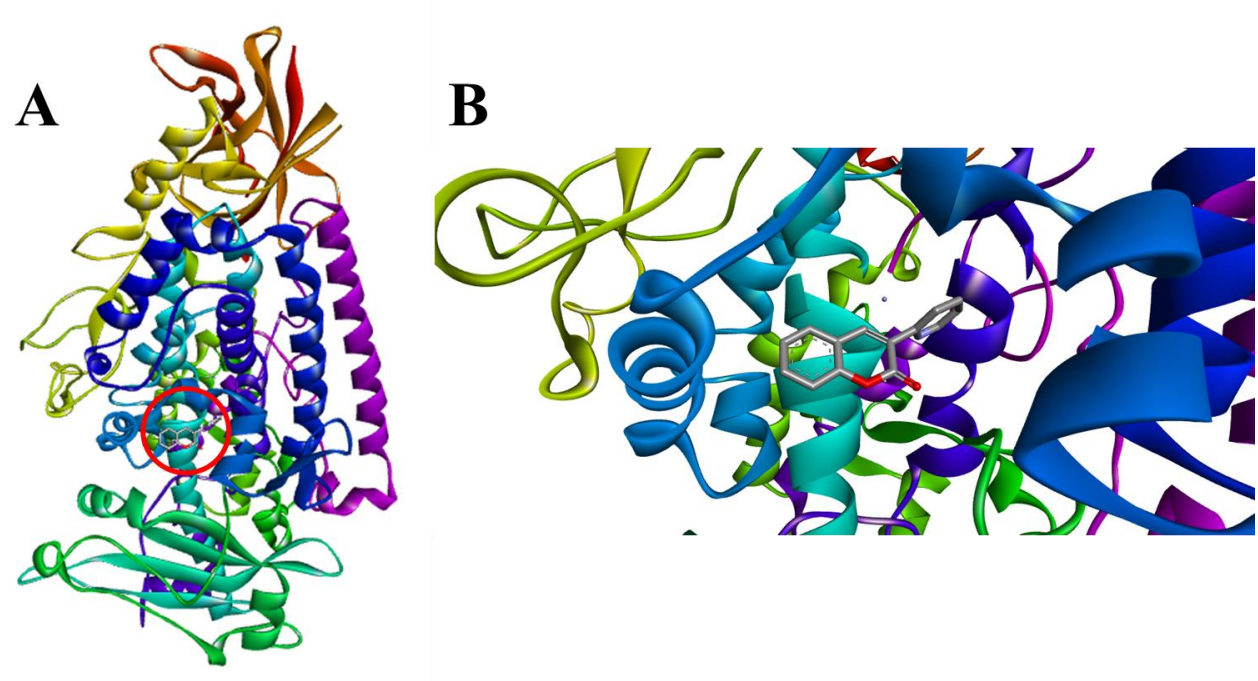

Fig. S32. Full view of the complex between the highest-ranking score of **1** and soybean lipoxygenase (**A**); zoom of the binding pocket occupied by the highest-ranking score of **1** and soybean lipoxygenase (**B**).

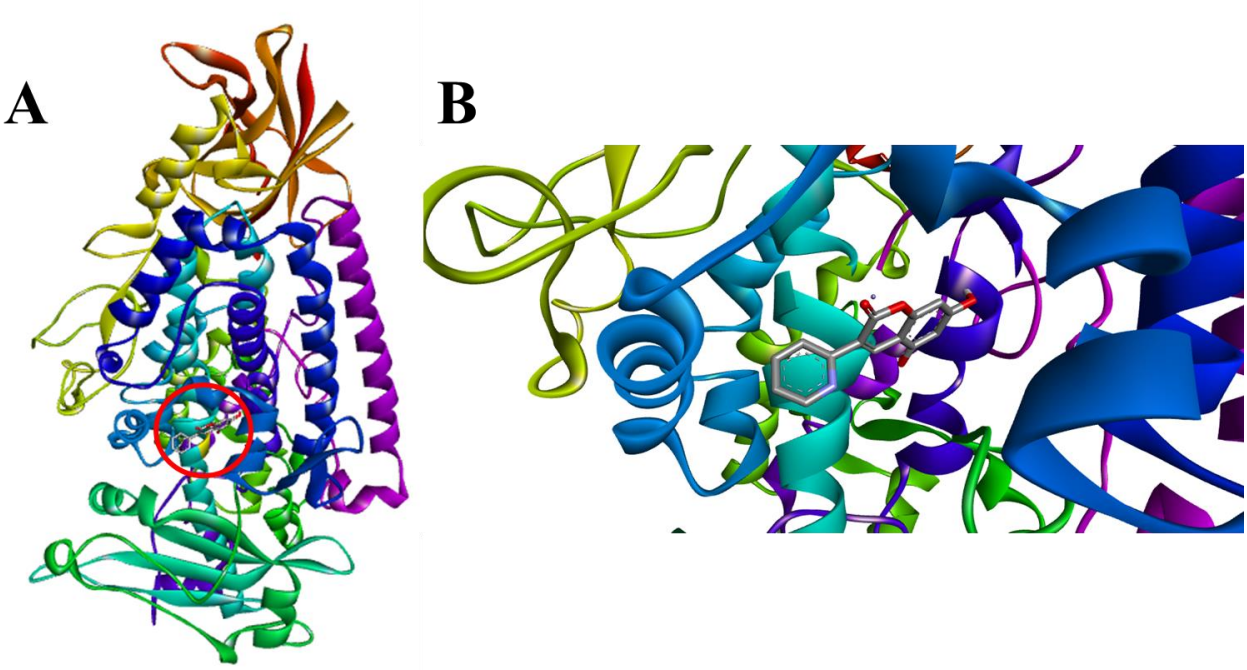

Fig. S33. Full view of the complex between the highest-ranking score of **3** (in its monoanionic form **HL**$^{-}$) and soybean lipoxygenase (**A**); zoom of the binding pocket occupied by the highest-ranking score of **3** (in its monoanionic form **HL**$^{-}$) and soybean lipoxygenase (**B**).

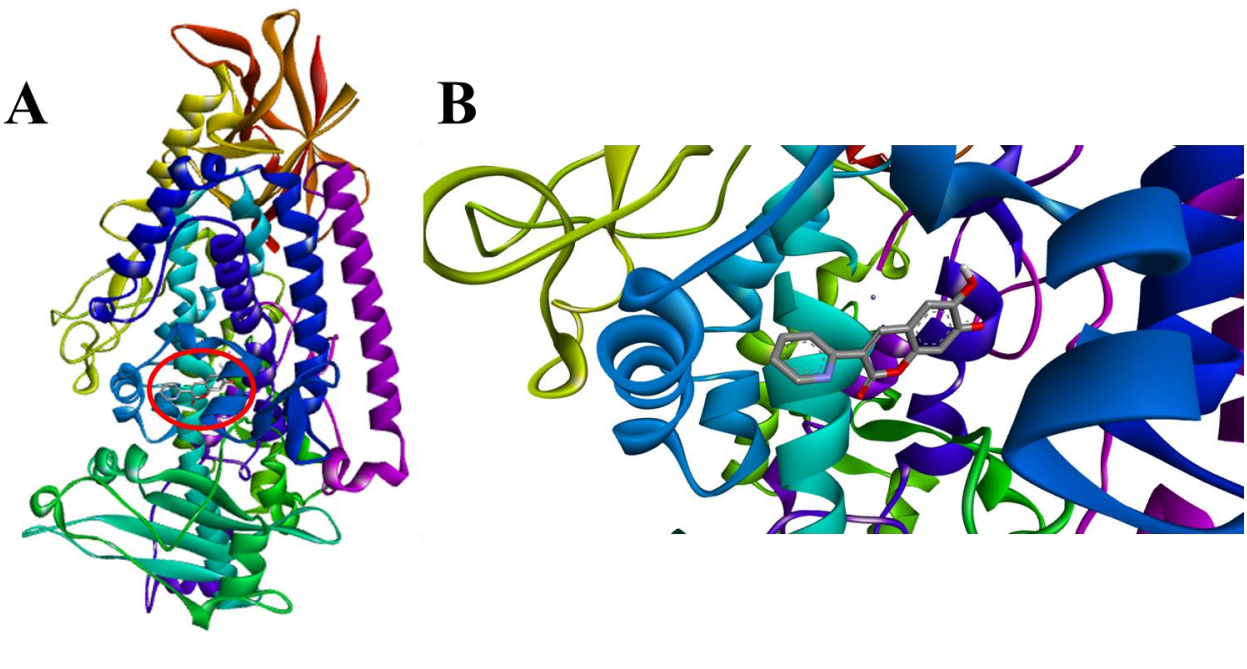

Fig. S34. Full view of the complex between the highest-ranking score of **4** (in its monoanionic form **HL**$^{-}$) and soybean lipoxygenase (**A**); zoom of the binding pocket occupied by the highest-ranking score of **4** (in its monoanionic form **HL**$^{-}$) and soybean lipoxygenase (**B**).

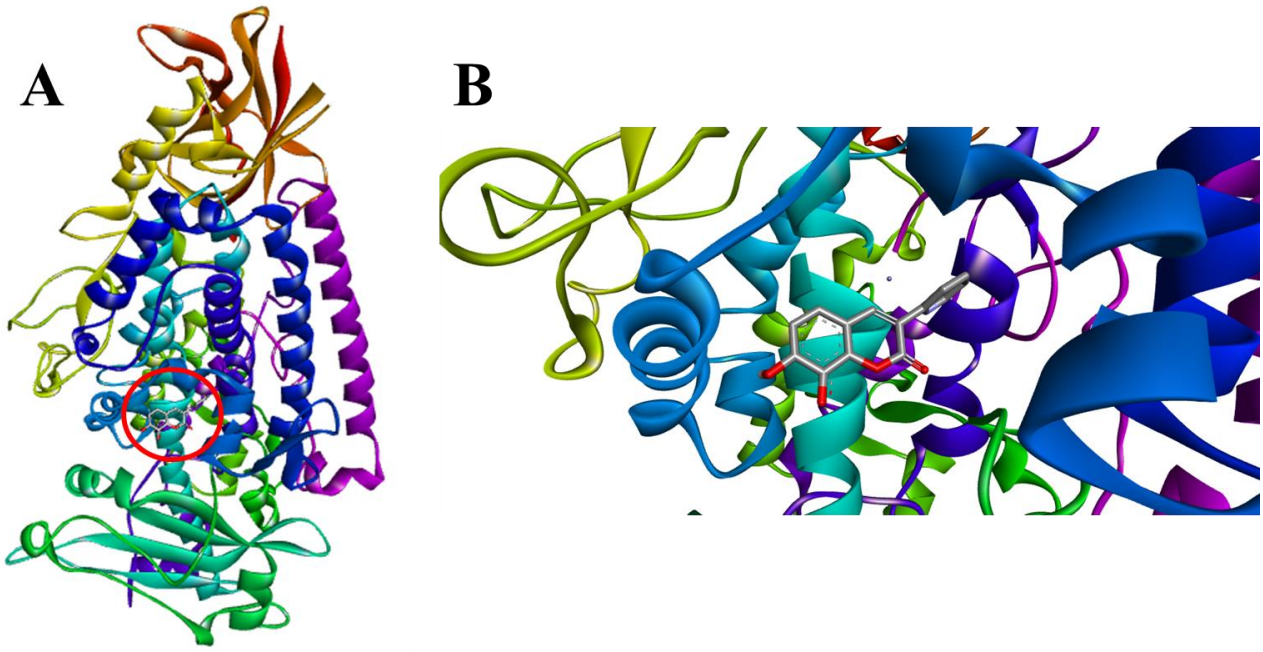

Fig. S35. Full view of the complex between the highest-ranking score of **5** (in its monoanionic form **HL**$^-$) and soybean lipoxygenase (**A**); zoom of the binding pocket occupied by the highest-ranking score of **5** (in its monoanionic form **HL**$^-$) and soybean lipoxygenase (**B**).

Table S1. Selected optimized bond distances (Å) and angles (°) for DFT-optimized structure of **1** (gas phase) and corresponding X-Ray structural parameters. Atom labelling scheme as in **Fig. 4A**.

1

	Structural parameters	**DFT-optimized**
C8-O2	1.370	1.348
O2-C7	1.374	1.378
C7-O1	1.204	1.201
C7-C6	1.476	1.466
C6-C5	1.488	1.482
C5-N1	1.355	1.339
N1-C1	1.324	1.321
C8-O2-C7	123.87	124.06

O2-C7-C6	117.25	116.62	
O2-C7-O1	115.74	116.04	
C7-C6-C5	120.55	121.43	
C6-C5-N1	114.21	114.97	
C5-N1-C1	117.96	119.02	
C7-C6-C5-N1	169.59	173.96	
C8-O2-C7-O1	179.77	179.68	

Table S2. Selected optimized bond distances (Å) and angles (°) for DFT-optimized structure of **2** (gas phase). Atom labelling scheme as in **Fig. 4B**.

2

C8-O2	1.345	**O2-C7-O1**	115.58
O2-C7	1.384	**C7-C6-C5**	121.53
C7-O1	1.201	**C6-C5-N1**	115.04
C7-C6	1.461	**C5-N1-C1**	119.07
C6-C5	1.481	**O3-C13-C14**	122.27
C5-N1	1.339	**O3-C13-C12**	116.95
N1-C1	1.321	**C7-C6-C5-N1**	179.64
O3-C13	1.348	**C8-O2-C7-O1**	179.99
O3-H6	0.961	**O3-C13-C12-C11**	-179.99
C8-O2-C7	124.02	**O3-C13-C14-C8**	179.99
O2-C7-C6	116.58		

Table S3. Selected optimized bond distances (Å) and angles (°) for DFT-optimized structure of **3** (gas phase). Atom labelling scheme as in **Fig. 4C**.

3

C8-O2	1.343	**C7-C6-C5**	121.52
O2-C7	1.386	**C6-C5-N1**	115.11
C7-O1	1.201	**C5-N1-C1**	119.09
C7-C6	1.459	**O3-C13-C14**	112.20
C6-C5	1.480	**O3-C13-C12**	116.46
C5-N1	1.339	**O4-C11-C9**	116.72
N1-C1	1.321	**O4-C11-C12**	122.49
O3-C13	1.348	**C7-C6-C5-N1**	179.34
O4-C11	1.347	**C8-O2-C7-O1**	179.92
O3-H6	0.962	**O3-C13-C12-C11**	-179.99
O4-H8	0.961	**O3-C13-C14-C8**	179.99
C8-O2-C7	124.39	**O4-C11-C12-C13**	-179.99
O2-C7-C6	116.49	**O4-C11-C9-C10**	-0.05

Table S4. Selected optimized bond distances (Å) and angles (°) for DFT-optimized structure of **4** (gas phase). Atom labelling scheme as in **Fig. 4D**.

4

C8-O2	1.348	**C6-C5-N1**	115.07
O2-C7	1.379	**C5-N1-C1**	119.07
C7-O1	1.202	**O3-C13-C12**	114.94
C7-C6	1.462	**O3-C13-C14**	123.84
C6-C5	1.481	**O4-C12-C11**	120.60
C5-N1	1.339	**O4-C12-C13**	120.18

N1-C1	1.321	**C7-C6-C5-N1**	177.95
O3-C13	1.357	**C8-O2-C7-O1**	179.96
O4-C12	1.352	**O4-C12-C111-C9**	-179.99
O3-H6	0.961	**O4-C12-C13-C14**	179.99
O4-H7	0.964	**O3-C13-C12-C11**	179.99
O3···H7	2.126	**O3-C13-C14-C8**	-179.99
C8-O2-C7	123.92	**O3-C13-C12-O4**	-0.01
O2-C7-C6	116.47	**O4-C12-C13-O3**	0.01
C7-C6-C5	121.47		

Table S5. Selected optimized bond distances (Å) and angles (°) for DFT-optimized structure of **5** (gas phase). Atom labelling scheme as in **Fig. 4E**.

5

C8-O2	1.350	**C6-C5-N1**	115.01
O2-C7	1.387	**C5-N1-C1**	119.09
C7-O1	1.200	**O3-C14-C13**	117.98
C7-C6	1.460	**O3-C14-C8**	123.20
C6-C5	1.481	**O4-C13-C14**	120.06
C5-N1	1.339	**O4-C13-C12**	119.70
N1-C1	1.321	**C7-C6-C5-N1**	179.58
O3-C14	1.356	**C8-O2-C7-O1**	179.97
O4-C13	1.345	**O4-C13-C12-C11**	-179.99
O3-H5	0.965	**O4-C13-C14-C8**	179.99
O3-H6	0.965	**O3-C14-C8-C9**	-179.99
O3···H6	2.174	**O4-C14-C13-C12**	179.99
C8-O2-C7	123.49	**O3-C14-C8-O2**	0.01

O2-C7-C6	116.23	**O3-C14-C13-O4**	-0.01
C7-C6-C5	121.27	**O4-C13-C14-O3**	0.01

Table S6. Selected atomic charges, calculated at Mulliken and NPA levels, of **1**. Atomic scheme as in **Fig. 4A.**

1

	Mulliken	**NPA**
O1	-0.318	-0.555
O2	-0.147	-0.422
N1	-0.233	-0.426

Table S7. Selected atomic charges, calculated at Mulliken and NPA levels, of **2**. Atomic scheme as in **Fig. 4B.**

2

	Mulliken	**NPA**
O1	-0.320	-0.557
O2	-0.152	-0.426
O3	-0.369	-0.643
H6	0.326	0.480
N1	-0.232	-0.423

Table S8. Selected atomic charges, calculated at Mulliken and NPA levels, of **3**. Atomic scheme as in **Fig. 4C**.

3

	Mulliken	**NPA**
O1	-0.321	-0.558
O2	0.148	-0.423

O3	-0.372	-0.626
O4	-0.372	-0.627
H6	0.328	0.481
H8	0.326	0.483
N1	-0.231	-0.427

Table S9. Selected atomic charges, calculated at Mulliken and NPA levels, of **4**. Atomic scheme as in **Fig. 4D.**

4

	Mulliken	**NPA**
O1	-0.325	-0.562
O2	-0.152	-0.424
O3	-0.429	-0.658
O4	-0.383	-0.633
H6	0.334	0.492
H7	0.335	0.491
N1	-0.231	-0.428

Table S10. Selected atomic charges, calculated at Mulliken and NPA levels, of **5**. Atomic scheme as in **Fig. 4E.**

5

	Mulliken	**NPA**
O1	-0.321	-0.557
O2	-0.223	-0.453
O3	-0.434	-0.662

O4	-0.374	-0.623
H5	0.347	0.506
H6	0.340	0.495
N1	-0.233	0.429

Table S11. Energy values (eV) of the frontier Molecular Orbitals of the studied compounds in gas phase, ethanol, and water at the DFT level (PBE0, def-2 TZVP).

compound	***gas***		***ethanol***		***water***	
	HOMO	**LUMO**	**HOMO**	**LUMO**	**HOMO**	**LUMO**
1	-6.64	-2.27	-6.73	-2.25	-6.78	-2.25
2	-6.34	-2.09	-6.38	-2.09	-6.39	-2.09
3	-6.21	-1.97	-6.29	-2.05	-6.29	-2.06
4	-6.18	-2.08	-6.21	-2.10	-6.21	-2.10
5	-6.30	-2.17	-6.30	-2.12	-6.30	-2.12

Table S12. Calculated thermochemical descriptors for the studied compounds in gas, ethanol, and water (DFT PBE0/def-2TZVP level). Atom labelling arrangement as in **Scheme 1**.

COMPOUND	***SITE***	***BDE (kcal/mol)***		
		Gas	**Ethanol**	**Water**
2	**7-OH**	84.66	85.72	85.75
3	**5-OH**	84.28	85.18	85.20
	7-OH	84.32	85.53	85.57
4	**6-OH**	84.12	82.43	82.43
	7-OH	74.26	77.28	78.03
5	**7-OH**	84.06	81.84	81.72
	8-OH	78.65	77.94	77.87
COMPOUND	***SITE***	***PA (kcal/mol)***		
		Gas	**Ethanol**	**Water**
2	**7-OH**	322.40	33.80	34.58
3	**5-OH**	326.10	33.47	34.23
	7-OH	325.32	33.63	34.44
4	**6-OH**	339.27	40.66	41.20
	7-OH	315.52	28.35	29.35
5	**7-OH**	329.27	34.87	35.52
	8-OH	328.33	33.39	34.02
COMPOUND	***SITE***	***ETE (kcal/mol)***		

		Gas	Ethanol	Water
2	**7-OH**	72.67	102.82	102.35
3	**5-OH**	71.56	102.58	102.15
	7-OH	72.38	102.78	102.32
4	**6-OH**	58.23	92.64	92.34
	7-OH	72.11	100.41	99.86
5	**7-OH**	68.24	97.85	97.38
	8-OH	63.81	95.43	95.02
COMPOUND	***SITE***	***SPLET (kcal/mol)***		
		Gas	**Ethanol**	**Water**
2	**7-OH**	395.07	136.62	136.93
3	**5-OH**	397.66	136.05	136.37
	7-OH	397.70	136.41	136.76
4	**6-OH**	397.50	133.30	133.54
	7-OH	387.63	128.76	129.21
5	**7-OH**	397.51	132.72	132.90
	8-OH	392.14	128.82	129.04
COMPOUND	***IP (kcal/mol)***			
	Gas		**Ethanol**	**Water**
2	174.69		128.92	126.10
3	171.14		126.46	123.67
4	171.16		124.82	121.93
5	173.58		127.34	124.41
COMPOUND	***SITE***	***PDE (kcal/mol)***		
		Gas	**Ethanol**	**Water**
2	**7-OH**	223.35	258.80	10.86
3	**5-OH**	226.51	260.72	12.71
	7-OH	226.56	261.07	13.09
4	**6-OH**	226.35	259.61	11.61
	7-OH	216.48	255.06	7.29
5	**7-OH**	223.86	256.50	8.50
	8-OH	218.57	252.53	4.64
COMPOUND	***SITE***	***SETPT (kcal/mol)***		
		Gas	**Ethanol**	**Water**
2	**7-OH**	387.04	387.72	136.96
3	**5-OH**	397.65	387.18	136.38
	7-OH	397.70	387.53	136.76
4	**6-OH**	397.51	384.43	133.54
	7-OH	387.64	379.88	129.22
5	**7-OH**	397.44	303.84	132.91
	8-OH	392.15	379.87	129.05